Tandem mass spectrometry in combination with ion mobility for characterization of cardiolipin molecular diversity

Novak, Angelo

Repository / Repozitorij:

Repository of the University of Rijeka, Faculty of Biotechnology and Drug Development - BIOTECHRI Repository

UNIVERSITY OF RIJEKA

DEPARTMENT OF BIOTECHNOLOGY

Graduate programme

"Biotechnology for the Life Sciences"

Angelo Novak

Tandem mass spectrometry in combination with ion mobility for characterization of cardiolipin molecular diversity

Master's thesis

Rijeka, September 2023.

UNIVERSITY OF RIJEKA

DEPARTMENT OF BIOTECHNOLOGY

Graduate programme

"Biotechnology for the Life Sciences"

Angelo Novak

Tandem mass spectrometry in combination with ion mobility for characterization of cardiolipin molecular diversity

Master's thesis

Mentor: Prof. Christian Andrew Reynolds, PhD

Rijeka, September 2023.

SVEUČILIŠTE U RIJECI

ODJEL ZA BIOTEHNOLOGIJU

Diplomski sveučilišni studij

„Biotehnološka istraživanja znanosti o životu"

Angelo Novak

Tandemska masena spektrometrija u kombinaciji s ionske pokretljivosti za karakterizaciju kardiolipinske molekularne raznolikosti

Diplomski rad

Mentor: Prof. Christian Andrew Reynolds, PhD

Rijeka, rujan 2023.

Master's thesis was defended on the 26th of September 2023.

In front of the Committee:

1. (Head of committee, title and full name)

2. (Committee member, title and full name)

3. (Mentor, title and full name)

This thesis has 56 pages, 18 figures, 1 table and 43 citations.

Abstract

Cardiolipin (CL), is a unique class of membrane phospholipids that is found almost exclusively in the mitochondrial inner membrane of eukaryotic cells. CL undergoes substantial remodelling through a highly conserved deacylation-transacylation pathway, and Barth syndrome is caused by a deficiency of the CL transacylase, Tafazzin (TAZ). Because of their unique structure, conducting an in-depth examination of the CL molecular diversity is challenging from an analytical perspective. However, when travelling wave ion mobility is combined with high-resolution tandem mass spectrometry (IM-MS/MS), a rapid and simple multidimensional characterization of the CL molecular diversity is made feasible due to CL separation from obscuring singly charged ion signals. Calculating the peak intensities that overlap the monoisotopic CL ions has been made easier thanks to the Python script used to automate the procedure. All of the IM-MS/MS-related parameters have been tuned to ensure CL separation and get optimum intensity, fragmentation, and quantitation from the samples. We demonstrate using IM-MS/MS that mutants of *Saccharomyces cerevisiae* lacking in CL remodelling (*Cld1ΔTaz1Δ*) exhibit a shift towards CL species with more saturated and shorter acyl chains. Furthermore, *Saccharomyces cerevisiae* mutant *Taz1Δ* also display a shift towards CL species with more saturated and shorter acyl chains but, the most relevant finding was that the MLCL/CL ratio has increased in a manner that is comparable to that seen in individuals with Barth syndrome. Our findings provide additional evidence that the CL profiles of different mammalian tissues are distinct from one another. In conclusion, IM-MS/MS is a method that is a powerful, robust and accurate tool when it comes to isolating CL species from complicated lipid samples and for identifying CL structural diversity.

Sažetak

Kardiolipin (CL) je jedinstvena klasa membranskih fosfolipida koji se mogu naći gotovo isključivo u mitohondrijskoj unutarnjoj membrani eukariotskih stanica. CL je podvrgnut značajnom preoblikovanju putem visoko očuvanog puta deacilacije-transacilacije, a Barthov sindrom je uzrokovan nedostatkom CL transacilaze (TAZ). Zbog njihove jedinstvene strukture, provođenje dubinskog ispitivanja molekularne raznolikosti CL-a izazovno je iz analitičke perspektive. Međutim, kada se pokretljivost iona putujućih valova kombinira s tandemskom masenom spektrometrijom visoke rezolucije (IM-MS/MS), moguća je brza i jednostavna višedimenzionalna karakterizacija molekularne raznolikosti CL zahvaljujući odvajanju CL od zamračujućih signala jednostruko nabijenih iona. Izračunavanje vršnih intenziteta koji preklapaju monoizotopne CL ione olakšano nam je zahvaljujući softveru Python koji smo koristili za automatizaciju postupka. Svi parametri povezani s IM-MS/MS podešeni su kako bi se osiguralo odvajanje CL-a i dobili optimalan intenzitet, fragmentacija i kvantifikacija iz uzoraka. Uspjeli smo pokazati pomoću IM-MS/MS da mutanti *Saccharomyces cerevisiae* kojima nedostaje CL remodeliranje (*Cld1ΔTaz1Δ*) pokazuju pomak prema CL vrstama sa zasićenijim i kraćim acilnim lancima. Nadalje, mutant *Saccharomyces cerevisiae Taz1Δ* također je pokazao pomak prema CL vrstama sa zasićenijim i kraćim acilnim lancima, ali je najrelevantnije otkriće bilo da se omjer MLCL/CL povećao na način koji je usporediv s onim viđenim kod pojedinaca s Barthovim sindromom. Naša otkrića pružaju dodatne dokaze da se CL profili različitih tkiva sisavaca međusobno razlikuju. Zaključno, IM-MS/MS je metoda koja je snažan, robustan i precizan alat kada je u pitanju izolacija vrsta CL iz kompliciranih uzoraka lipida i za identifikaciju strukturne raznolikosti CL.

Table of contents

1. Introduction

1.1 Cardiolipin

Mitochondria are regarded as the cell's powerhouse, providing almost all of the energy necessary for cell metabolism through the process of oxidative phosphorylation. Several more cellular physiological processes, including autophagy, redox signalling, programmed cell death, and Ca2+ homeostasis, are also regulated by these organelles. The outer mitochondrial membrane and the inner mitochondrial membrane (IMM) are the two membranes that characterise mitochondria and a phospholipid is a lipid molecule that serves as the primary component of the cell membrane (1). Several phospholipid species may be found in the IMM, but the one we are interested in is cardiolipin (CL). CL [bis-(1,2-diacyl-sn-glycero-3-phospho)-1'-3'-sn-glycerol] is a distinct family of glycerophospholipids made up of two phosphatidyl moieties connected by bridging glycerol and four acyl chains. Cardiolipins, in the IMM, are mostly common in crista and are essential for several of the organelle's functions as it accounts for approximately 15% of total mitochondrial phospholipids (2).

1.1.1. Cardiolipin synthesis

Phospholipid biosynthesis is a remarkably conserved pathway in all eukaryotes. *De novo* synthesis of CL occurs in mammalian organs, through the cytidine-5-diphosphate-1,2-diacylsn-glycerol pathway. The mechanism starts with glycerol-3-phosphate acyltransferase (GPAT) adding an acyl group from acyl-CoA to the sn-1 position of glycerol-3-phosphate to generate 1-acyl-sn-glycerol-3-phosphate, also known as lysophosphatidic acid. The lysophosphatidic acid, a product of GPAT is then acylated at the sn-2 position by 1-acyl-sn-glycerol-3-phosphate acyltransferase (AGAPT) to generate 1, 2-diacyl-sn-glycerol-3-phosphate (phosphatidic acid or PA). Bound to PRELID1, PA travels across the intermembrane gap to reach the inner membrane, where it is processed by TAMM41 into CDP-diacylglycerol

(CDP-DG) (3). The next transfer of the activated phosphatidyl group from CDP-DAG to the sn-1 position of sn-glycerol-3-phosphate by phosphatidyl glycerol phosphate (PGP) synthase to create PGP is the committed step in the CL synthesis pathway. The newly generated PGP is then degraded by a phosphatase to create phosphatidyl glycerol (PG) in the next phase of the pathway. At the pathway's last step, PG accepts an activated phosphatidyl group from another CDP-DAG molecule to produce the newly formed CL. This process is conducted by CL synthase (CLS), an enzyme found only in the IMM (4). The CL synthesis pathway (and remodelling) is shown in (Figure 1).
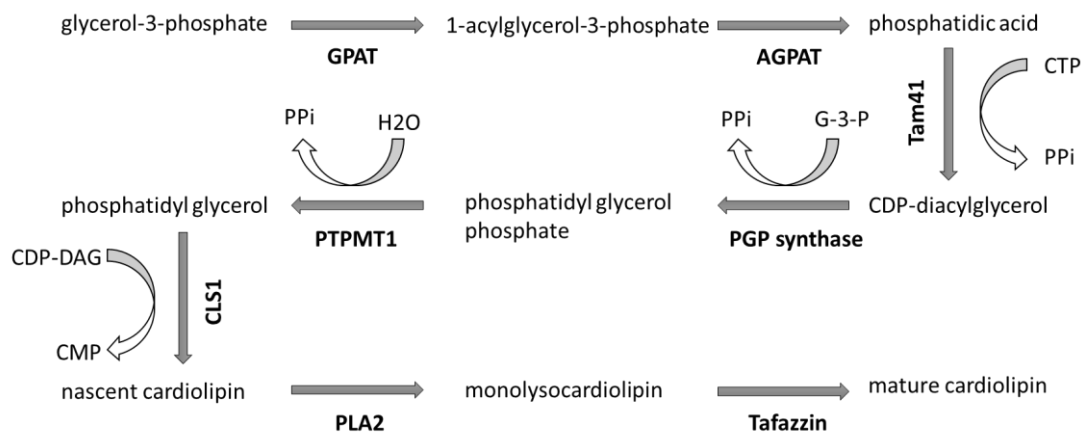
Figure 1. Synthesis and remodelling pathway of cardiolipin. See text for abbreviations.

1.1.2. CL remodelling

Because CLS has limited acyl substrate specificity and the acyl composition of mature CL differs significantly from that of *de novo* synthesis species, remodelling has been proposed to occur. Shortly after *de novo* synthesis, CLs obtain the tissue-specific acyl groups required for their functions. That is the fatty acid (FA) exchange that results in mature CL species with long unsaturated chains. CL remodelling occurs in two phases and is started by phospholipases such as Cld1 in yeast and iPLA2-VIA47 in the fruit fly. They deacetylate CL with higher affinity towards more saturated acyl chains, to

monolysocardiolipin (MLCL) which acts as an acyl acceptor in the next process. The complete molecular makeup of the upstream lipase responsible for CL deacylation *in vivo* in humans, however, is still mostly unknown (5). According to Hsu et al. (2013) human phospholipases, including iPLA2β, iPLA2γ, cPLA2, and especially secreted phospholipase A2 (sPLA2) may deacylate CL to MLCL *in vitro* (6). Finally, a FA from a phospholipid is reacylated to an MLCL by Tafazzin (TAZ), which results in the production of a new CL and due to its affinity, it shifts acyl composition towards unsaturation. The CL remodelling pathway is shown in (Figure 2). However, CL fatty acyl arrangement is not random; for instance, in heart tissue, the content is dominated by a single CL species, CL $(18:2)_4$, but in brain tissue, longer acyl chains (20:4 and 22:6) in CLs were observed. As a result, it is hypothesised that CL molecules with varying acyl chain compositions are functionally unique and that the molecular shape of CL is tailored to the needs of its host cell. However, the processes that create and maintain tissue-specificity in CL compositions are still mostly unknown (7).
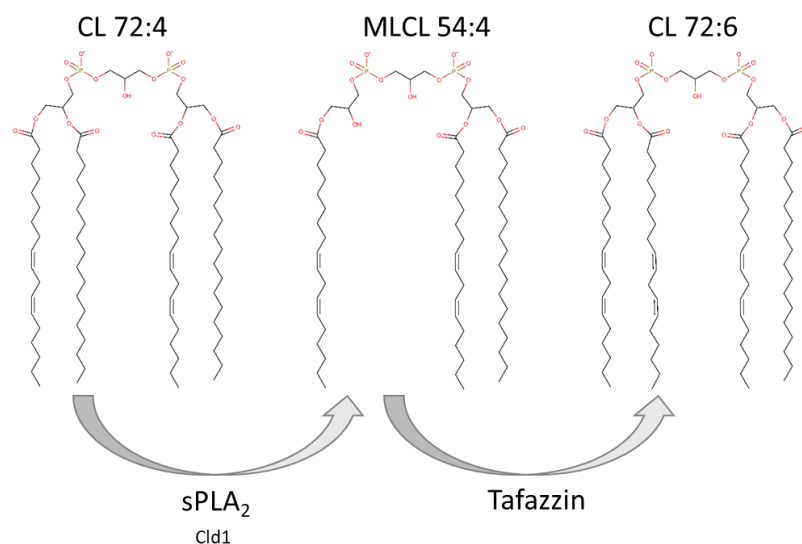

Figure 2. Cardiolipin remodelling pathway. Deacylation of CL is thought to be done by the sPLA2 enzyme in humans or the Cld1 enzyme in yeast. Reacylation of CL is done by Tafazzin both in humans and yeast. (Figure made in MarvinSketchu according to Vetica et al.(8))

1.1.3. Barth syndrome

In 1983, Dr Peter Barth made the first discovery of the rare genetic disorder known as Barth syndrome (BTSH). BTHS is the only illness in humans where both a decrease in CL content and alterations in its molecular acyl composition are the primary cause of pathogenesis. Cardiomyopathy, skeletal myopathy, neutropenia, growth retardation, and increased urine excretion of 3-MGCA are the most well-known symptoms of the condition. Additional health issues include pubertal growth impairment, delayed motor tasks, and recurring bacterial infections as a result of neutropenia. According to the Barth Syndrome Foundation Registry, the prevalence ranges from 1 in 300,000 to 400,000 live births and with no known racial or ethnic preferences to exist (9). BTHS is caused by a mutation in the TAZ gene, which consists of 11 exons and is located on Xq28. In terms of evolution, the TAZ sequence exhibits remarkable conservation. The transacylase enzyme tafazzin, which is encoded by the gene TAZ, remodels freshly generated CL with tissue-specific acyl chains to produce the mature CL required for proper mitochondrial function. The molecular characteristics of BTHS include an irregular cristae shape in the mitochondria, accumulation of MLCL, and a sharp decline in unsaturated CL species. Unfortunately, it is unclear exactly how these factors affect the pathogenesis of BTHS. Missense mutations and tiny insertions or deletions make up the majority of mutations, although a small percentage of individuals had significant exon deletions or full gene deletions. This condition is incurable since it is a genetic disorder, however, it may be controlled with drugs and therapies for heart failure (10).

1.1.4. CL structure

Because of the contrast between a small hydrophilic head group and a large hydrophobic body, the CL molecule often displays a cone-like shape. Because of its cone shape, CL can segregate into regions of negative membrane curvature, where it aids in the development and maintenance of IMM cristae (11). If the phosphate groups are charged, a significant repulsive force is created, and charged CL molecules take on a cylindrical shape and form bilayers with the phosphate groups spaced farther apart in response to the electrical repulsion (12). This characteristic might allow CL to take in varying degrees of curvature, which improves the stability of cristae formation in mitochondria. Importantly, the FAs in CL influence phase formation. Short, saturated chains promote cylindrical molecules with zero curvature, while long, unsaturated chains favour molecules with a cone shape (negative curvature) (13).
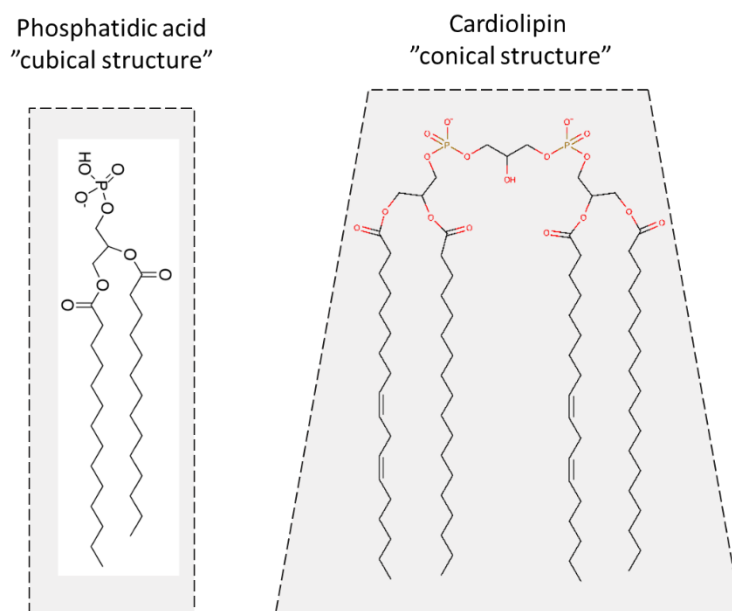

Figure 3. Cardiolipin unique shape. Cubical structure of classic phospholipids such as phosphatidic acid in comparison to the more conical structure of CL. (Figure made in MarvinSketchu according to Vetica et al.(8) and Thakur et al.(14))

1.1.5. CL functions

Many mitochondrial carrier proteins, including ADP/ATP carrier (ANT), phosphate carrier, pyruvate carrier, and carnitine/acylcarnitine translocase, interact with CL and require it for proper function. Only in the presence of CL 72:8 was the ANT activity found to be at its peak, whilst other CL species and phospholipids were ineffectual in catalysing the ANT activity. Moreover, CL interacts with all electron transport chain (ETC) complexes and is essential for their structural stability and enzymatic activity (11). Distinct CL binding sites have been identified in complexes I, III, and IV, while complexes III and IV even include several bound CLs, which are necessary for their stability and functional activity. When these bound CLs are removed, almost all of the activity is lost, and the subunits of these complexes separate. When the CLs are reinserted, the quaternary structure is stabilised, and full activity is restored. Additionally, cytochrome c and cardiolipin interact to push cytochrome c closer to the ETC, that way, the electron transport from complex III to complex IV is accelerated (15).

Cytochrome c (cyt c) is a mitochondrial protein that transfers electrons in the ETC and, more importantly, the release of cyt c from mitochondria to the cytosol is a crucial step in the activation of the apoptotic cascade. It has been found that CL binds to cyt c at two distinct sites: electrostatic interactions that contribute to cyt c's electron transfer, and hydrophobic interactions between one of CL's unsaturated acyl chains and a cyt c residue. During apoptosis, CL moves from the IMM to OMM, where it forms a peroxidase-active cyt c/CL complex. This action destabilises the cyt c's tertiary structure and the CL oxidizes by the peroxidase activity of the complex. Cyt c has a lower affinity for oxidised CL, allowing it to be released from mitochondria into the cytosol during apoptosis (15)(16).

Mitochondria are a key source of reactive oxygen species (ROS) which are produced when electrons leak out onto molecular oxygen during ETC electron transport. The primary locations of O^- production are thought to be

Complexes I and III. CL molecules are particularly vulnerable to oxidative damage by these radical species because of their large proportion of unsaturated acyl chains and their proximity in the IMM to the source of ROS generation. As a result, CL may serve as a significant target for antioxidant defence techniques through the method of constant remodelling of acyl chains, especially already oxidized ones (15).

1.2. Model organisms

Various model organisms have been studied to understand the mechanisms and significance of cardiolipin remodelling. Some of these organisms include mouse (*Mus musculus*), yeast (*Saccharomyces cerevisiae*), zebrafish (*Danio rerio*), and fruit fly (*Drosophila melanogaster*)**.** These model organisms provide important new understandings of the mechanisms and effects of cardiolipin remodelling in many cellular environments (17). What defines the remodelled composition of CL species is now at the heart of the dispute. The study has shown that human TAZ generates CL with a *Drosophila*-like pattern when synthesised in TAZ-deficient *Drosophila*, suggesting that the transacylation process is controlled by the host environment (the spectrum of accessible FA) rather than the enzyme (18). There have also been several significant discoveries using yeast model. The deletion of Cld1 prevents CL remodelling in yeast, resulting in the presence of only *de novo* synthesized, saturated CLs. Surprisingly, the deletion of Cld1 also saves the yeast TAZ-deficient growth fault. In contrast to *Cld1ΔTaz1Δ* double mutants, which had a normal overall CL level, decreased unsaturation, low MLCL/CL, and normal growth, the *Taz1Δ* mutant had a low overall CL level, reduced unsaturation, and high MLCL/CL. These findings imply that saturated CL may perform numerous unsaturated CL tasks and that the negative consequences of TAZ mutation are caused by increased MLCL/CL or decreased total CL (19). Another study was conducted in *Saccharomyces cerevisiae* and *Drosophila melanogaster* where a variety of deletions and knockdowns, including carriers, membrane homeostasis proteins, fission-fusion proteins, cristae-shape controlling proteins, and complexes I-V, to

determine the process that imposes acyl specificity on CL remodelling *in vivo*. Only the complexes of oxidative phosphorylation (OXPHOS) affected the CL composition. The overall disruption of the OXPHOS system, rather than any single complex, changed CL composition and decreased its half-life. In *Drosophila* muscles, knocking out OXPHOS had the same impact on CL as knocking out TAZ, including a shift in CL composition and the build-up of MLCL. Consequently, the formation of OXPHOS complexes causes CL remodelling, which leads to CL stability (20).

1.3. Mass spectrometry

As mentioned previously, people with BTHS have high levels of MLCL and a high ratio of MLCL to CL, which is often used as a sensitive diagnostic marker. More and more evidence indicates that abnormal CL metabolism and structure are linked to pathologies in humans, such as neurological disorders, cancer, heart, and metabolism problems. It is important to comprehend the variety of tissue-specific CL acyl chain structures to build analytical methods and understand changes in CL species under pathological disorders. The most popular method for quantification of CLs at the moment is mass spectrometry (MS), which is becoming more and more available and advanced (21). MS is an analytical technique that correctly calculates the molecular masses of individual compounds and atoms. The main advantages of this approach are its specificity, sensitivity, and capacity to analyse real-world samples. Ionization, ion separation based on the mass over charge (m/z) ratio, and ion detection are all necessary components of mass spectrometric analysis. For these purposes, a mass spectrometer consists of an ion source, a mass analyser, a detector, a data system, a vacuum system, and electronic control components. A mass spectrum is created by measuring, amplification, and displaying the ion current caused by these mass-separated ions. The data is shown as a mass spectrum, which is a plot of the m/z values on the x-axis vs the abundances on the y-axis (22).

1.3.1. Ionization

The first step is ionization, which turns analyte molecules into gas-phase ions. While several ionisation methods have been developed over the years, electrospray ionisation (ESI) and matrix-assisted laser desorption/ionization (MALDI) have emerged as the two most used ones. In ESI, ions are produced at atmospheric pressure by passing a solution-based sample through a tiny capillary with an internal diameter of ~0.1mm while a voltage is applied to the tip of the capillary of around 2-6 kV. ESI of a sample solution makes an aerosol of charged droplets and depending on the polarity of the applied voltage, the charged droplets include solvent and analyte molecules with a net positive or negative charge. The charge intensity on the surface of the droplet progressively rises and ions eventually separate from the solvent that surrounds them, and they enter the spectrometer's mass analyser. ESI is a very 'soft' approach since there is very little fragmentation, a useful technique when injecting biological molecules of large molecular mass. Unfortunately, one of ESI's shortcomings is that a sample is continually consumed, so a portion of the sample is wasted (22)(23). Unlike ESI, which produces analyte ions continuously, ions in MALDI are formed by irradiating a sample with a pulsed laser. The sample is co-crystallized with a solid matrix that can absorb the laser's wavelength of light. Typically, the sample and matrix are combined on a probe that is put into the vacuum system, and the resulting gas-phase ions are guided onto the mass analyser after irradiation (22)(24).

1.3.2. Mass analyses

Secondly, the molecular ions and their charged fragments are then separated and subjected to mass analyses based on their m/z (mass-to-charge) ratios. The different types of mass analyser measure ions in different ways. Time-of-flight (TOF) mass spectrometers are perhaps the fundamentally simplest mass analysers as ions are divided depending on their velocity. Theoretically, the ions are created in the ion source at the

same time and location and are then propelled into the TOF drift tube at a given voltage (for instance, 1-20 kV). The lower m/z ions reach greater velocities than the higher m/z ions because all ions with the same charge get the same kinetic energy following acceleration. The accelerated ions pass through a given distance, before impacting the detector. Hence, when the ion is created, the m/z of the ion may be calculated by timing how long it takes to reach the detector (25). However, the most accurate results are achieved with more advanced TOF equipment that has a reflection. After passing through one flight distance in a reflectron TOF, the ions enter an electrostatic mirror, which then spins them around and sends them down a second flight distance to the detector. The reflectron's job is to make up for little variations in the velocities of ions with the same m/z. As a result, the reflectron improves TOF spectrometry's resolution (22).

The quadrupole has likely been the most popular mass analyser throughout the years. To separate ions, a quadrupole analyser employs a mass filter that combines radio frequency alternating current and direct current voltages. Four parallel rods make up the quadrupole. An equal amount of negative DC voltage is applied to the two rods, while the positive DC voltage is delivered to the two opposite rods. The quadrupole rods' combined DC and RF potentials may be configured to only pass ions of a certain m/z ratio. All other ions will crash with the quadrupole rods and never make it to the detector because they lack a steady pathway through the quadrupole mass analyser (22). A TOF analyser counts the number of ions of all m/z in each measurement, in contrast to the quadrupole analyser, which counts ions of just one mass-to-charge ratio in each measurement. There is a required period per ion for full-spectrum quadrupole scans. As a consequence, the measurement is quite time-consuming. However, the one area in which the quadrupole still excels relative to the other instruments is in quantification (26).

1.3.3. Tandem mass spectrometry

Since CL has four acyl chains, it has a huge range of potential molecular configurations that may be represented by a given molecular mass of CL. For instance, a CL with one 18:2, two 18:1, and one 16:1 acyl chain, would have the same molecular formula ($C_{79}H_{144}O_{17}P_2$) and precise mass of 1426.9879 u as a CL with one 18:1, one 20:4, and two 16:0 acyl chains. Tandem mass spectrometry (MS/MS) is, therefore, a necessary additional step analysis process. Using MS/MS provides confirmation of CL and additional important information about the structure characteristics. MS/MS consists of two or more mass analysers connected in series, separated by a fragmentation cell, such as collision-induced dissociation (CID), electron-transfer dissociation (ETD), photodissociation, etc. The first analyser is used to isolate ions with a certain m/z, afterwards subjecting these ions to fragmentation. The resultant product ions are then separated and identified via a secondary mass analyser (27). After cardiolipin fragmentation, additional structure information is gained. Three distinctive areas of the resulting spectra are characteristic of each cardiolipin species: the diacylglycerol phosphate fragment, the monoacylglycerol phosphate fragment, and the FA fragment. With this, it is possible to confirm if any signal at a certain m/z is CL and which acyl chains it is made of (28).

1.3.4. Singly charged vs doubly charged

The advantages and disadvantages of comparing cardiolipin species that are singly charged vs doubly charged by MS have been examined in several studies. Sparagna et al. used singly charged cardiolipin molecular ions to detect and quantify CL molecular species in rat cardiac mitochondrial lipid extracts. The API 2000 mass spectrometer and ESI ion source were utilised to produce the spectra, which showed that the single-charged molecule was predominant with 95% singly charged [M-H] and 5% doubly charged CL ions. When CL was analysed using the QSTAR quadrupole time-of-flight instrument under the same solvent conditions, a greater fraction of the

doubly charged species (around 25%) was found. Using a third type of mass spectrometer, the API 3000, the percentage of doubly charged CL was even higher, at 40%. The study of singly charged CL species, according to the authors, enables a finer separation of their isotopic peaks and may provide more precise relative abundance data for molecular species that are only separated by 2 or 4 amu (29). Because of this, one benefit of MALDI-MS CL detection is that all CL species are identified as single-charged ion species (30). Nonetheless, Valianpour and his colleagues used ESI-MS product ion analyses of doubly charged cardiolipin molecular ions to identify and measure cardiolipin molecular species in platelet lipid extracts from BTSH patients, as single-ion species made up only less than 0.5% of all ions under ideal experimental conditions (31). Moreover, doubly charged cardiolipin species may provide more structural details because they are more likely to generate fragment ions that show make-up of FA side chains. These doubly charged ions share a mass range (670-780 m/z) with several abundant singly charged glycerophospholipid ions, which might be a major disadvantage if they can't be separated (32). Consequently, the individual study objective, the accessible equipment, and the sample type all influence whether to analyse singly charged or doubly charged cardiolipin species by mass spectrometry (MS).

1.3.5. Separation

As previously stated, doubly charged ions have the same mass range (670-780 m/z) as many of the abundant singly charged glycerophospholipid ions including phosphatidic acid, phosphatidylethanolamine, and phosphatidylglycerol. The majority of research on CLs is performed with the liquid chromatography-mass spectrometry (LC-MS) technique to separate the CL from this abundant and easily ionized lipid species (33). Using this method, lipid mixtures are dissolved in a liquid mobile phase, which allows for the separation of individual lipid components based on their polarity and molecular interactions with the mobile phase and stationary phase tightly

filled onto a column. The advantages of the LC-MS method are several stationary phases, column settings, and elution solvents to choose from. When the separated analytes elute from the column, the mass spectrometer can measure their distinctive retention times (21). Two major types of HPLC can be employed for the detection and quantification of CLs, reversed-phase HPLC (RP-LC) and normal-phase HPLC (NP-LC). In the NP-LC the mobile phase is made up of nonpolar solvents (such as hexane and heptane), while the stationary phase is polar. Adsorption of polar components of a solute (such as phospholipid head groups) onto a polar stationary phase provides the basis for the binding of the analytes, whilst nonpolar components of the solute play little to no role. This means, very hydrophobic species may not be separated with NP-LC, such as cardiolipin, based on the hydrophobic nature of the FA side chains. On the other hand, in RP-LC, the silica microparticles that make up the nonpolar stationary phase are complexed with hydrophobic or mixed ligands, such as C30, C18, or C8, while the mobile phase is water-soluble and polar. The retention mechanism involves hydrophobic interactions between the solution and stationary phase hydrophobic ligands. Therefore, the more hydrophobic CLs elute later from the column than the less hydrophobic ones (34).

Using RP-LC-MS, Garrett et al used four quantitative CL synthetic standards to quantify the CL levels in macrophages. These standards were selected because they are not isobaric with other CL compounds or negatively charged molecules with comparable retention periods. Each standard was diluted into mobile phase A at a different concentration to describe the behaviour of the CL standards using LC-MS. As anticipated, the CL 57:4 standard eluted first with an estimated 8.5-min retention time, followed by the CL 61:1 standard at 10.66 min, the CL 80:4 standard at 12.95 min, and the CL 86:4 standard at 13.79 min, which demonstrates a separation. However, the extracted ion intensity peak areas for the CLs 61:1, 80:4, and 86:4 were linear for 1 pmol to 50 pmol injected into the column, and the peak area of the EIC for the CL 57:4 was linear only for 1 pmol to 25 pmol.

Meaning, the mass spectrometry response of the four standards decreased linearly with increasing chain length. The difference between the intensity produced by the same amount of CL 57:4 and CL 86:4 is almost 9 times. As different cardiolipin species are eluted during chromatographic separation, they are in different solvent solutions during ionization which causes this matrix effect, representing a serious limitation in quantification (33). There has been a development in recent studies by Oemer et al., where an absolute quantification was achieved by linear regression analysis with externally measured dilution series of commercially available standards (CL $(14:0)_4$ and CL $(18:1)_4$). Ionization efficiencies between CL $(14:0)_4$ and CL $(18:1)_4$ were highly similar where they have shown that the matrix effect caused by separation was improved (35). However, they have not shown if there still might be a matrix effect present in CL with longer acyl chains as they elute later when a solvent solution is more different. Another problem with the LC-MS separation of CLs is shown in the reverse-phase system used by, Garrett et al where CLs also elute with phosphatidylethanolamine species. For example, the doubly-charged CL 72:5 (m/z 726.603) has the exact mass retention time on the column as the single-charged 36:2 plasmenyl-ethanolamine (PLE), (726.544 m/z). Yet, neither the monoisotopic (MI) $[M-H]1^-$ PLE ion nor the ion with one $^{13}C_1$ atom (PLE-$^{13}C_1$) overlaps the CL-$^{13}C_1$ 72:5, m/z 727.029. Using only this approach, by examining the CL-$^{13}C_1$ ion can they distinguish CLs from other singly charged ions. In addition, two peaks can be seen when the MI mass 72:5 CL is extracted from the total ion current chromatograph. The larger peak, which appears at 11.23 min, is associated with singly charged ions, while the smaller side peak, which appears at 12.58 min, is associated with 72:5 CL. Meaning, only, if the mass of the 72:5 CL-$^{13}C_1$ ion is extracted, then a peak at 12.62 min is isolated and can be used for quantification (33).

Another method, direct infusion mass spectrometry of lipid samples without previous chromatographic separation is referred to as shotgun lipidomic. While it lacks the chromatographic resolution separation of LC-MS

techniques, it may be utilised to conduct several mass spectrometry studies when coupled with a powerful mass spectrometer. However, this classical shotgun method has a few limitations that make it hard to use in cardiolipin and lipidomic quantification. Ion suppression is the most often criticised one because it may have an impact on ion production, limiting dynamic range, detection precision, and quantification accuracy. Ion suppression may make it harder to study some classes of lipids, such as those that are rare or hard to ionise. The traditional shotgun lipidomic may also make it difficult to find artifactual peaks in the spectrum that are caused by the ion source. Even if the ESI source is thought to be soft, there is always in-source fragmentation in ESI-MS. Certain ion source-generated artifactual peaks may be found in the obtained mass spectrum when a characteristic fragment of a class is recognised. Thus far, this method cannot discriminate between artifactual peaks (36). Han X. et al. have shown that they had created an extended shotgun lipidomics technology that could accurately analyse around 30 individual cardiolipin molecular species directly from lipid extracts of mouse heart. When using a triple quadrupole (QqQ) to analyse, the lower resolution m/z of the double-charged ion and its isotopic peaks need deconvolution for accurate quantification (37). Also, this QqQ MS-based lipidomic method requires the pre-selection of specific ions for analysis of CLs. Recently, the strategy of MS/MS[ALL] data-independent acquisition (DIA) methods has been proposed by Gao et al. to overcome this shortcoming by recording all the fragments in isolation windows with various m/z widths (38). The primary drawback of MS/MS[ALL] is that it eventually results in the loss of information on the interactions between precursors and fragments, making the identification of CLs more difficult (39).

1.3.6. Ion mobility

Because of the diversity of lipids and their sidechains, it is not always possible to determine the lipids with absolute certainty based only on their mass and fragmentation patterns as several species have similar atomic compositions and are isobaric. Ion mobility spectrometry (IMS) is one of the technologies that has been developed to make it possible to identify such isobaric mixtures (21). IMS is a technique employed in gas-phase analysis to determine the velocity at which ions travel through a tube filled with buffer gas under the influence of a uniform electric field. The deceleration of ions as a result of collisions with buffer gas will occur to a limited extent, leading to distinct drift times. IMS permits the separation of isobaric ions in the gas phase based on their shape, charge, and size (40). In this study, we used the Synapt G2-S high-resolution tandem mass spectrometry in combination with travelling-wave ion mobility (IM-MS/MS), which allowed the molecular diversity of CL to be characterised in a simpler and faster multidimensional way than previously described techniques. Due to their higher speed, double-charged ions are completely separated from single-charged ions using mass spectrometry, which lets us solve the problem of separating isomeric lipids effectively.
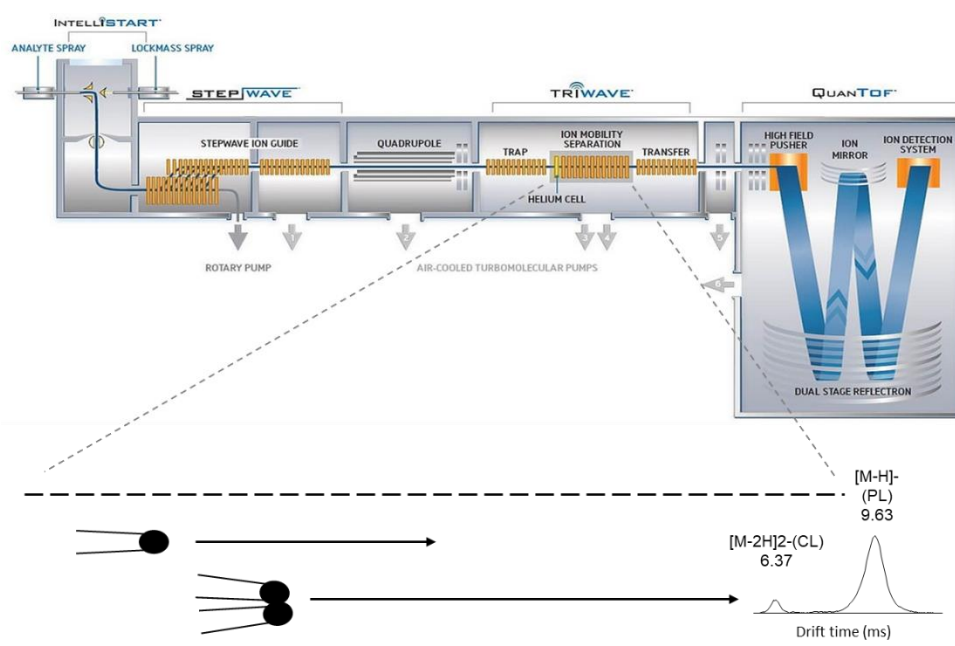

Figure 4. Schematic of the SYNAPT G2-S mass spectrometer (41)**.**

2. Objectives of the work

The main aim of this work is the development and optimization of the method using tandem mass spectrometry in combination with ion mobility for accurate quantification and characterization of cardiolipin molecular diversity. In addition, the aim is to develop a robust method for recognizing and correcting MI intensity CL peaks and visualising CL profiles using a Python script. The aim is also to compare CL profile diversity between CL remodelling pathway mutants and WT and also to compare CL profile diversity between different rat organ tissues (brain, heart, liver).

This research hypothesises that using ion mobility, perfect separation of doubly charged CLs from obscuring, more abundantly singly charged ions is possible in a much more robust, accurate and sensitive way than in research conducted using different methods. The second hypothesis is that by comparing *S. cerevisiae* yeast WT and its CL remodelling pathway mutants C*ld1ΔTaz1Δ* and *Taz1Δ*, it can be shown what effect these missing enzymes have on CL profile and their importance in regulating CL homeostasis. The third hypothesis is that different organ tissue of the same mammalian will have different CL profiles due to specific organ function requirements.

3. Materials and Methods

3.1. Chemicals and standards

Ethanol, (LC-MS hyper grade), methanol (LC-MS hyper grade), acetonitrile (ACN) (LC-MS hyper grade), triethylamine (LC-MS grade), agar, peptone from meat, yeast nitrogen base without amino acids, yeast extract, uracil, histidine, leucine, methionine were ordered from Sigma Aldrich (St. Louis, MO, USA). D (+)- glucose anhydrous, chloroform (LC-MS hyper grade), water (LC-MS hyper grade) and isopropanol (LC-MS hyper grade) were ordered from VWR chemicals (Radnor, USA). CL standards $(14:0)_4$, $(16:0-18:1)_2$ and $(18:1)_4$ were ordered from Avanti Polar Lipids (Alabaster, USA).

3.2. Making media

Two different media were used. YPD is made using 10g of yeast extract, 20g of peptone, 20g of glucose and 20g of agar, filled up to 1 L with distilled water. SMD was made using 6.7g of yeast nitrogen base, 20g of glucose, 20g of agar, and 20 mL of Minimal AA/B mix, filled up to 1 L with distilled water. Minimal AA/B mix is made with (0.5g of uracil, 0.125g of histidine, 0.75g of leucine, and 0.25g of methionine filled up to 250 mL with distilled water).

3.3. Growing yeast

Yeast species *S. cerevisiae* is an organism we used to obtain lipid extracts for CL detection optimization and to explore differences in CL composition in different mutants related to CL remodelling. S. cerevisiae cell lines: *Taz1Δ, CldΔTaz1Δ* and isogenic wild type (WT) control cell lines were provided to us by Prof. Miriam Greenberg from Wayne State University in Detroit, Michigan, USA.

All of our yeast strains were plated on yeast extract peptone dextrose (YPD) agar media and incubated at 30˚C. For WT strains at normal growth temperatures on rich media, this takes 2 - 4 days. Yeast cells should be white-yellow. Next, a single colony from the plates was used to inoculate a liquid preculture in 10 mL synthetic minimal media (SMD) media. Cells are grown in a flask, or tube, in an incubator while shaking at ~ 230 rpm. Flasks

should be no more than 1/3 full so there is oxygen present. The purpose of the preculture is to let the cells reach the log phase when they are most competent and to allow us to start all cultures with the same number of cells. This was done by measuring the optical density (OD) of precultures using a spectrophotometer and by calculating the volume of media that needs to be added to make a culture containing a specific number of cells. When they entered the log phase, yeast cells from preculture were taken and cultured in the same media at the same OD value (in this case, 0.05 A600). To find out how many hours each strain is required to reach each phase, the OD of liquid cultures was measured at different time points so that a growth curve could be generated. Using the growth curve, the time each strain required to exit the lag phase and enter the log and stationary phases of growth was determined. When the cultured cells reached the desired stage, they were centrifuged for 3 minutes at 3500 rpm and washed 3 times with distilled water by centrifugation after which the cell pallet was used for lipid extraction.

3.4. Lipid Extraction

After a pallet from 1ml of 50 OD yeast cells was prepared, lipid extraction was made as previously described by Knittelfelder and Kohlwein with some modifications of protocol. We did not use glass beads to homogenise cells, instead, we used sonicator Bandelin Sonopuls, while the rest of the protocol is the same. The sonicator settings were set Am= 92% / total run time= 6min / Pulse= 30sec sonication 60sec rest. Lipid extracts were subsequently resuspended in a 1ml infusion right before injection in mass spectrometry was intended. Note: the lipid extract is best to use within 7 days to remove a risk of lipid degradation.

3.5. Mass spectrometry

The ion mobility mass spectrometry instrument we use is an SYNAPT G2S; it is a powerful analytical tool developed by Waters Corporation. It is equipped with a high-stability quadrupole mass analyser combined with a high-performance acceleration TOF mass analyser, named QuanTof. The

acquisition system was programmed to repeatedly accumulate 200 TOF spectra throughout the ion mobility drift time (~10 ms). In addition to QuanTof, it has TriWave technology that combines ion mobility with dual collision cells; front Collision Induced Dissociation (CID) and rear Electron Transfer Dissociation (ETD). By adding ion mobility separation to traditional mass spectrometry, the SYNAPT G2S can provide faster and better separation of CLs from singly charged ions, resulting in more accurate and reliable results. The region of mobility is occupied by nitrogen gas. The ions undergo their initial passage through a helium cell located at the forefront of the mobility region. The utilisation of a helium cell enhances the efficacy of ion transmission into the mobility region while also reducing the likelihood of ion fragmentation through kinetic cooling upon entry into this region of elevated pressure.

Moreover, this specific placement of the ETD cell makes the SYNAPT G2S perfect for analysing CLs structure using the MS/MS method. Because the ion mobility separation is happening before the ion fragments are generated from the CL precursor ion in the ETD, all CL fragment ions have the same drift time as a precursor ion. We are therefore sure that CL fragments ions are also separated from fragments ions originating from singly charged ions. This provides additional information on the structure and identity of the CL. ESI was used as an ion source for most of the experiment, however, some work also includes work on an ion source Nanoflow. MassLynx v4.1 software was used to control the instrumental parameters setup of the experiments and for the visualisation of chromatograms. The Driftscope software was used for the visualisation and manipulation of ion mobility data.

3.6. IMS-MS/MS method development

All of the CL standards and lipid extractions were injected into the mass spectrometry in a solution made of 50%ethanol, 30% acetonitrile, 20% miliQ and 0.1mM TEA at a flow rate of 15 µL/min with ESI and 2 µL/min with Nanoflow.

3.6.1. Optimization of CL ionization

Different concentrations (1.0, 0.5, 0.25, 0.1, 0.05, 0 µmM) of triethylamine (TEA) were made with 0,16 µmM of CL standard $(14:0)_4$ to determine which TEA concentration produced the highest CL intensity signal. Each sample was injected into mass spectrometry and each concentration was recorded 3 times, of which we took the average to determine the best intensity signal.

3.6.2. Preparing standard dilutions

Linear regression analysis was done with externally measured dilution series of commercially available standards $(14:0)^4$, $(16:0-18:1)^2$ and $(18:1)^4$ CL. One 1ml with 1mM of all 3 standards was prepared in LC grade ethanol and sonicated for 10 minutes. From that 1mM standards, dilutions (0.00128, 0.0064, 0.032, 0,16, 0.8, 4 µM) were made, and injected into mass spectrometry. Dilutions were injected from the lowest to highest concentration to eliminate the possibility of carryover. The washing process between every sample was made starting with 100% methanol then 50% methanol/ 50% miliQ and finishing with 100% miliQ at a flow rate of 30 µL/min.

3.6.3. Optimization of CL separation

By adjusting various instrument parameters, the distance of ion separation using IMS can be varied. Nitrogen gas flow, helium gas flow, and wave height were found to affect the distance at which ions are separated. Nitrogen gas flow was tested at 30, 40, 50, 60, 70, 80, and 90 mL/min, and helium gas flow was tested at 60, 80, 100, 120, 140, 160, and 180 mL/min. Wave velocity setting influences were measured at 1400, 1500, 1600, 1700, 1800, and 1900 V. Moreover, on the same instrument parameters, settings were altered to check whether they might influence the CL intensity signal. To test this, the intensity signal of CL 66:4 (685.4 m/z), 68:4 (699.4 m/z), 70:4 (713.4 m/z), 68:4 (727.4 m/z) was measured in triplicate. Helium DC was also measured at 30, 50, 70, 90, 110, 130, and 150 V as it has been shown to cause a change in the CL ion intensity.

3.7. Monoisotopic CL intensity correction

An additional complication when quantifying CLs is the significant overlap of the MI $[M-2H]^{2-}$ CL ions with the $^{13}C_2$ and $^{13}C_4$ isotope ions of CL species with the same number of carbons. For example, the $^{13}C_2$ isotope ion of CL 64:4, overlaps with the MI ion of the CL 64:3, while the $^{13}C_2$ isotope ion of the CL 64:3 and $^{13}C_4$ isotope of CL 64:4 overlap with the MI ion of CL 64:2. Because of the large number of carbons in CL the $^{13}C_2$ isotope ion can be more than 50% of the peak area of the most abundant isotope and, therefore, cannot be disregarded.

MassLynx software was used to predict isotopic distributions for all possible CLs (based on the number of carbons and double bonds). Using these predicted isotopic distributions, we calculated what is the ratio of the $^{13}C_2$ isotope compared to MI (factor-1) and the $^{13}C_4$ isotope compared to MI (factor-2) of that CL. Then the equation was made to calculate the correct intensity of each MI CL. The equation is *Corrected intensity = [Intensity at X m/z] – [Intensity at X-1±0.025 m/z * factor-1] - [Intensity at X-2±0.05 m/z * factor-2].* Because there are a lot of CL possibilities, we have developed a Python script to automatically calculate from the spectrum intensity list what intensities are matching to certain CL and correct their MI intensity.

3.8. Fragmentation

After being corrected for intensity, the intensities that matched a specific CL are fragmented. MS/MS is carried out using an ETD cell and ion mobility of precursor/product ions was collected in 200 asynchronous time segments followed by TOF measurement. The transfer cell was set at 28 V. Most frequently, glycerol, FA, monoacylglycerol-phosphate, and both singly and doubly charged MLCL, are the fragment ions that are present following the fragmentation of the CL. However, CLs with the same m/z can have structurally distinct FAs despite having the same total length of carbon chains and the same number of double bonds. As a result, fragmentation enables us to characterise the precursor CL ion's structural properties based

on the fragment FA ions. In conclusion, it can be confirmed that the precursor ion is CL if the majority of the fragments mentioned are present and if the double bonds and carbon numbers of the FAS can add up to the total double bonds and carbon numbers of the CL.

3.9. Signal-to-noise ratio calculations

Dilution series of commercial CL standard $(14:0)_4$ (0.00128, 0.0064, 0.032, 0,16 µM) were injected and had their spectra recorded in triplicate with and without IMS deconvolution. The intensities of different $(14:0)_4$ CL concentrations were averaged by its triplicate and this result represented a signal intensity of certain CL concentration. The total spectra of each dilution in both cases (with and without IMS) were then copied into the Microsoft Excel sheets. The intensity signal from CL $(14:0)_4$ and its isotopes were removed from the rest of the total spectra which was then averaged. This averaged spectrum was averaged again by 3 repeats and this result represented a noise intensity in spectra. The signal-to-noise ratio was then simply calculated by dividing the signal by the noise of a certain CL concentration.

4. Results

4.1. Ion mobility-mass spectrometry

As was said earlier, one of the most challenging aspects of identifying and quantifying doubly charged CLs through the use of mass spectrometry is isolating CLs from the extremely numerous singly charged ions. The direct injection spectrum of rat liver lipid extract has demonstrated that the strongest intensities of singly charged ions fully mask the intensity signals of doubly charged CL species; the greatest peak has an intensity of 3,24e5. This is evident in inset spectra in the 730–750 m/z region, where there is a 1 m/z difference between each peak, indicating that the ions are singly charged. The CL 74:x and 76:x m/z ranges fall within this range; however, they cannot be distinguished (Figure 5a). When we investigated the IMS method's ability to separate ions, the two-dimensional plot that was generated revealed that doubly charged ions travel more quickly through nitrogen gas than singly charged ions do, allowing for rapid and effective spectrum deconvolution (Figure 5b). The extracted spectrum from the two-dimensional plot of doubly charged ions has a completely different appearance than the direct injection spectrum. Unlike raw spectra, the deconvoluted spectrum has the highest intensities between 650m/z and 750 m/z which correspond to the m/z range of doubly charged CLs. The strongest peak in this spectrum has an intensity of 3,98 e-4, which is 10 times less than the biggest intensity in the direct injection spectrum indicating that the unwanted, obscuring intensities are removed. Moreover, the inset spectra confirm the presence of only doubly charged ions as the difference between each peak is 0.5 m/z and CLs 74:x and 76:x can now be clearly appreciated (Figure 5c).

Using 0,0064µM standard $(14:0)_4$ CL, we wanted to compare the raw and IMS spectrum (Figure 6a). When comparing the two spectra it is clear that the raw spectrum has much bigger background noise than the IMS spectrum and the IMS spectrum also has much better looking peaks and even CL 56:0 third isotope ($^{13}C_3$) at 620.9 m/z can be appreciated. Still, it can be noted

that in the raw spectrum, the MI of 56:0 CL ion intensity is 1.20e4, while in IMS deconvoluted spectrum the intensity of MI CL 56:0 is 443, which indicates that using IMS results in overall ion intensity lost. We confirm this by comparing of intensity signal of different CL 56:0 concentrations (0.00128, 0.0064, 0.016, 0.032 μM) without and with IMS deconvolution, where the ion intensity in concentration curve with IMS is constantly almost ten times lower than without IMS (Figure 6b.). However, without using IMS deconvolution, the ion intensity signal is much bigger, but the noise background is also much lower. By calculating signal to noise ratio at low CL 56:0 concentrations (0.00128, 0.0064, 0.016μM), it is clearly shown that IMS deconvolution provides around 20-30 times better signal-to-noise ratio than without IMS (Figure 6c).
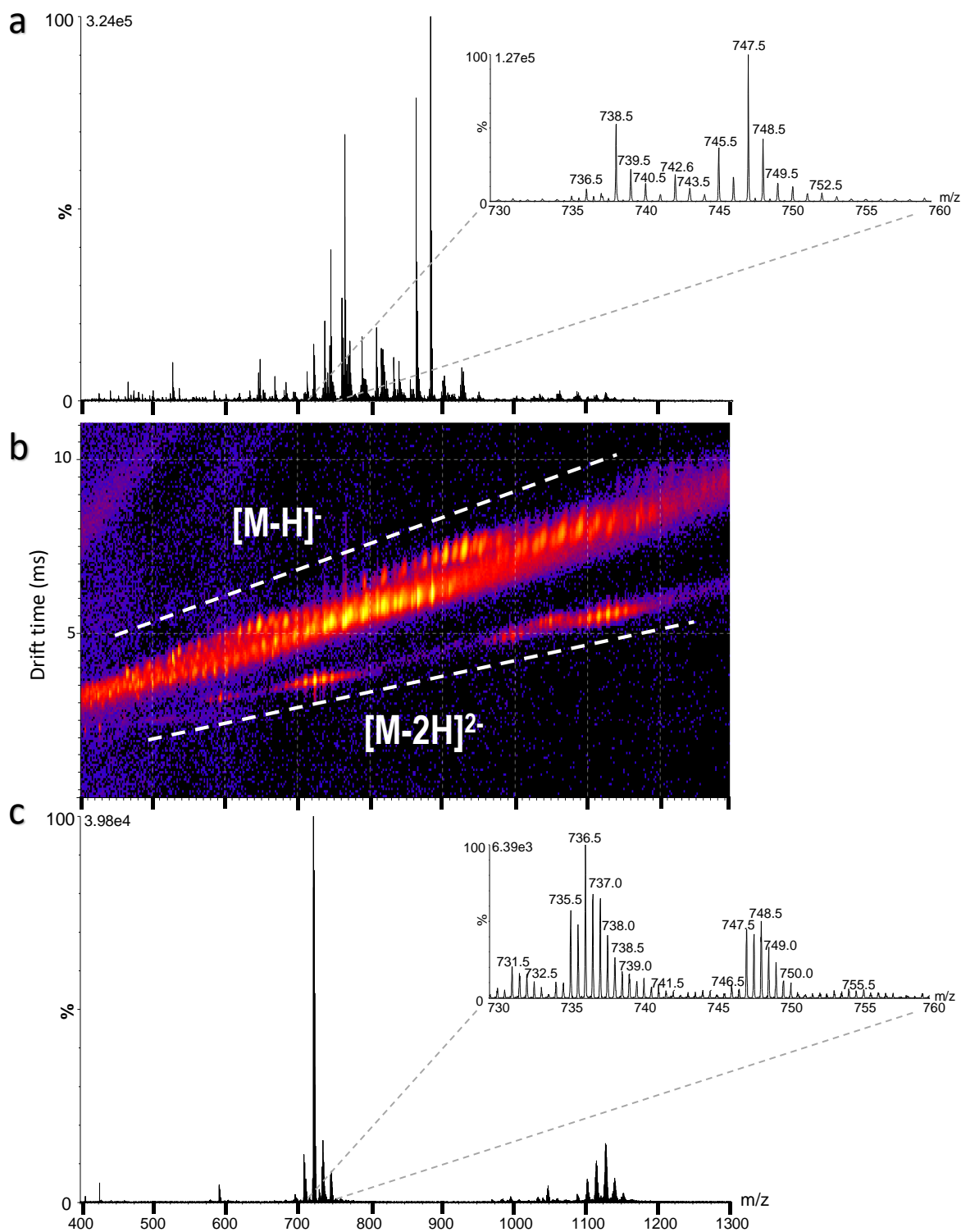
Figure 5. IMS spectrum deconvolution of lipid yeast extract. (a) The raw MS spectrum of yeast extract. **(b)** Two-dimensional plot of IMS drift time vs m/z. Separation of doubly charged ions $[M-2H]^{2-}$ from singly charged ions $[M-H]^-$ in Drift-scope software. **(c)** The spectrum of separated and extracted doubly charged ions from a two-dimensional plot. The inset

spectra highlight the extensive isotopic overlapping of doubly charged and singly charged ions which are overcome using IMS deconvolution.
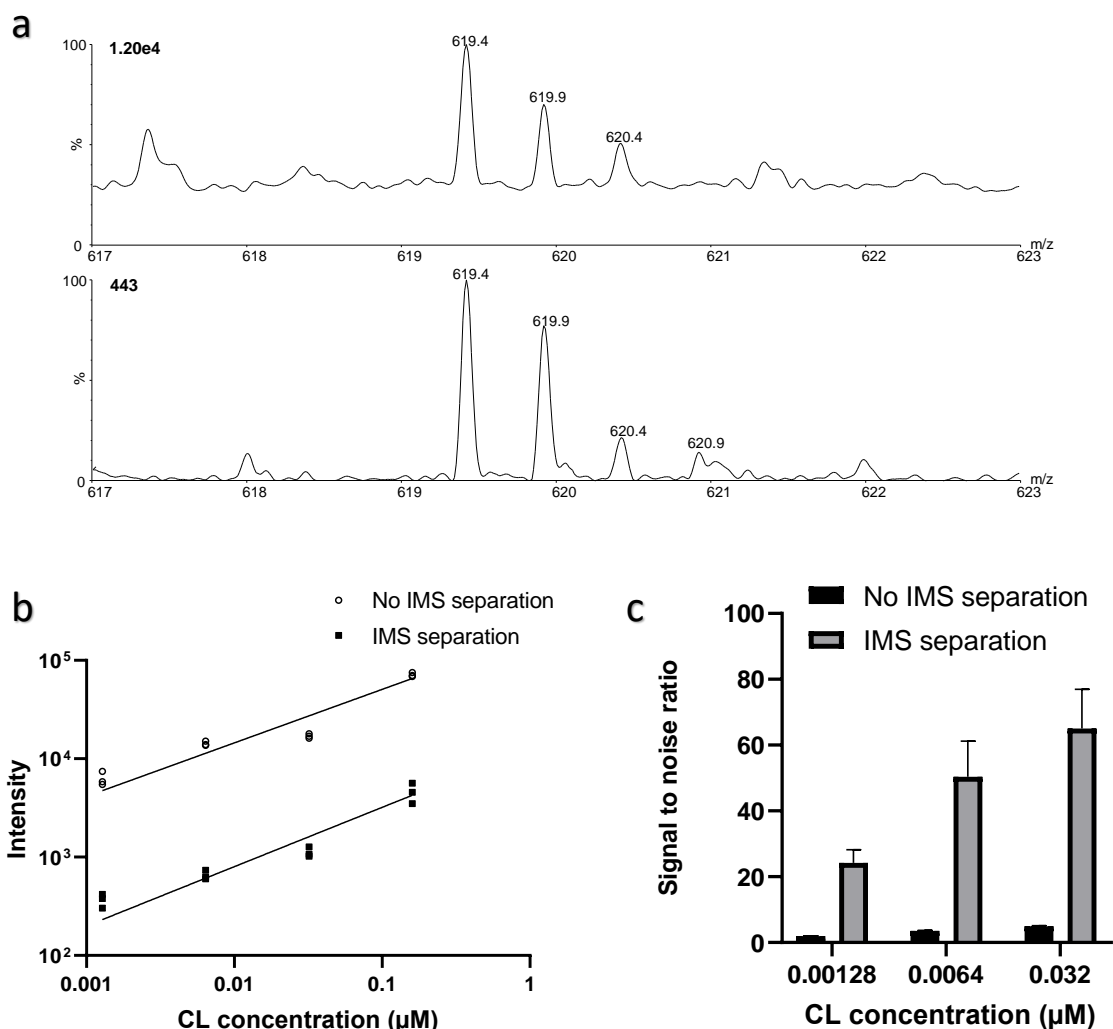
Figure 6. IMS deconvolution results in weaker overall signal intensity but a higher signal-to-noise ratio. (a) Comparison of raw spectra and IMS deconvoluted spectra with 0.016μM standard CL $(14:0)_4$. **(b)** Intensity signal comparison between without and with IMS deconvolution of different standard CL $(14:0)_4$ concentrations (0.00128, 0.0064, 0.016, 0.032 μM). **(c)** Signal-to-noise difference between without and with IMS deconvolution of standard CL $(14:0)_4$ concentrations with error bars. (b) and (c) are measured in triplicate.

4.2. Isotopic deconvolution

Isotopic distribution refers to the relative abundance of different isotopes of an element in a given sample. It is represented by the percentage of each isotope present in the sample. Table 1. shows the predicted isotopic distributions for the CL 64:4 calculated using the isotopic distribution calculator of the Waters MassLynx software. The $^{13}C_2$ isotope ion is 35.7% and $^{13}C_4$ is 2.9% of the intensity peak area of the MI ion. These calculated peak areas are used for the quantification (Table 1).

Table 1. Isotope distribution for 64:4 cardiolipin.

Isotope	CL 64:4 Relative abundance
MI	1
$^{13}C_1$	0.812
$^{13}C_2$	0.357
$^{13}C_3$	0.114
$^{13}C_4$	0.029

The now separated and extracted spectra have only doubly charged ions present with selected spectra showing the range of 64:4 CL (Figure 7. a). This spectrum is obtained from *Cld1ΔTaz1Δ* double mutant lipid extract. The peak at 671.4 m/z corresponds to the MI of CL 64:4, peak at 672.4 m/z corresponds to the MI of CL 64:3, peak at 673.4 m/z corresponds to the MI of CL 64:2, and peak at 674.4 m/z corresponds to the MI of CL 64:1.

However, before determining the intensity in these MI peaks, intensity peak correction has to be done because of isotopic overlapping. 64:x CLs isotopes overlapping is shown in Figure 7b where each colour represents the predicted distribution of isotopes and their intensity based on the intensity of MI. Four is the maximum number of double bonds in CLs the yeast can biosynthesise with provided growth media. Therefore, MI of 64:4 CL does not have any CLs with the same number of carbons and more double bonds that might result in its isotopic overlapping. However, it can be easily seen that $^{13}C_2$ of 64:4 CL and MI of 64:3 CL have the same masses causing the two different CL to have the peak overlap. Likewise, $^{13}C_2$ of 64:3 CL and MI of 64:2 CL overlap, but the $^{13}C_4$ of 64:4 CL also has the same mass, and it overlaps. Unfortunately, $^{13}C_4$ of 64:4 CL cannot be appreciated as the intensity is too small to be shown in the spectra. At 674.4 m/z, besides the MI of 64:1 CL, both intensities of $^{13}C_2$ of 64:3 CL and $^{13}C_2$ of 64:3 CL can be easily seen to cause an overlap on the same peak. Knowing that MI of CLs have the same masses as both $^{13}C_2$ of CL with one more double bond and $^{13}C_4$ of CL with two more double bonds, we developed a straightforward equation to quantify MI peak intensities. The equation used: *corrected intensity = [Intensity @ X m/z] − [Intensity @X-1±0.025 m/z * factor-1] - [Intensity @X-2±0.05 m/z * factor-2]*, where factor-1 represents a relative abundance of $^{13}C_2$, and factor-2 represents a relative abundance of $^{13}C_4$. Structures of mentioned CLs are shown in Figure 7c and the percentage of 64:x CLs in this *Cld1ΔTaz1Δ* yeast extract is shown in Figure 7d.
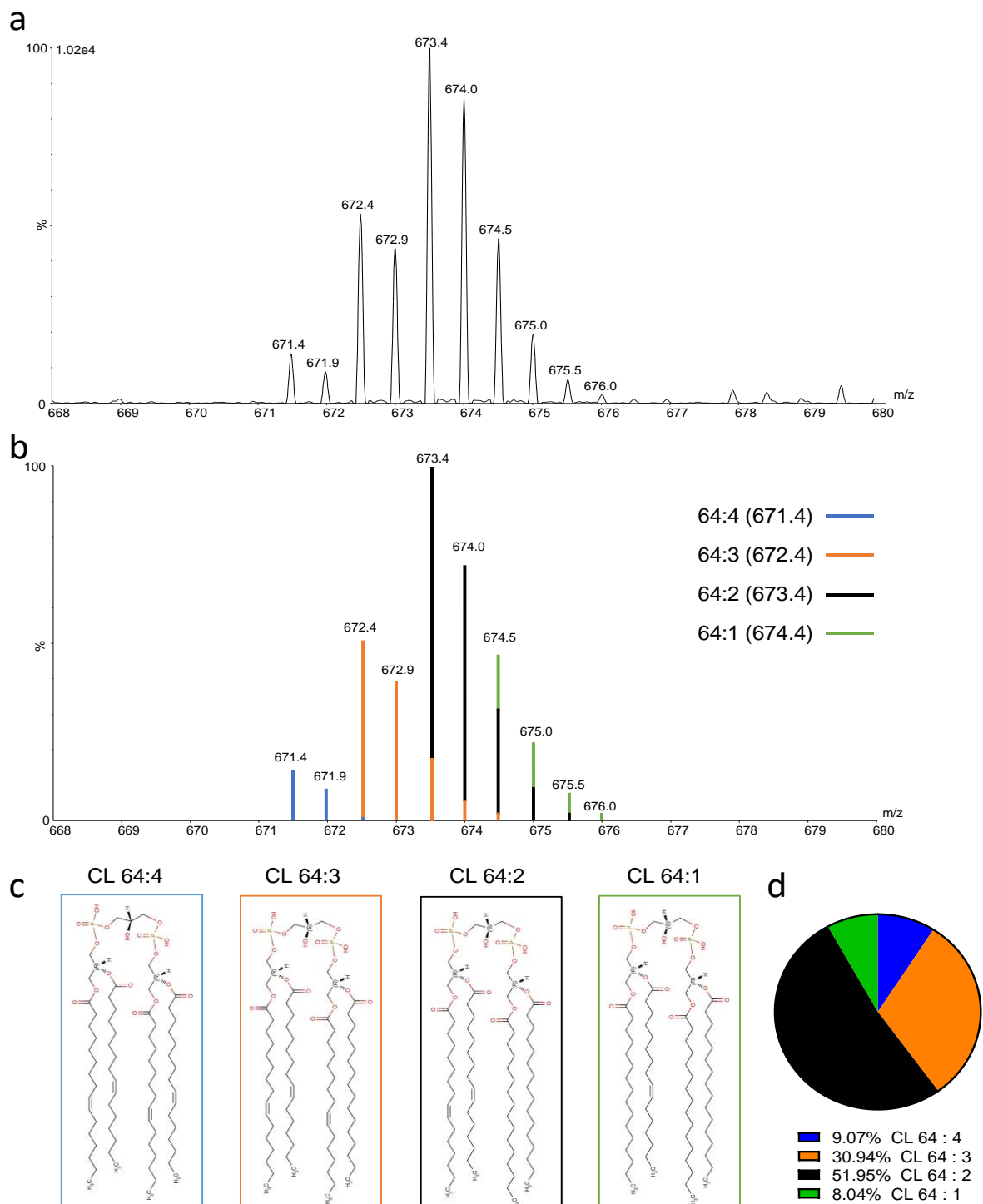
Figure 7. Isotopic deconvolution of monoisotopic CLs. (a) Extracted, IMS- deconvoluted WT yeast spectrum of [M-2H]$^{2-}$ CLs 64:x. **(b)** Intensity peak overlapping correction of CL 64:x MI masses based on predicted isotopic distribution. **(c)** Structures of identified CL 64:x species. **(d)** Percentage of MI mass intensities of each CL 64:x after isotopic correction.

4.3. MS/MS analysis of cardiolipins

To confirm whether an intensity peak matched with a certain m/z from the CL database is originating from a CL ion or rather some other doubly charged ion with the same m/z, the MS/MS method of that peak has to be made. Using a quadrupole, only ions with a certain m/z of interest can be selected to pass through it and consequently, both singly and doubly charged ions enter a quadrupole. Luckily, this issue is overcome because the IMS deconvolution happens before fragmentation resulting in the precursor and product ion having the same drift times. Using IMS drift time, fragment ions originating from the doubly charged $[M-2H]^{2-}$ CL precursor ion with a drift time of ~6ms (white box) are cleanly separated from those originating from the singly charged $[M-H]^-$ precursor ion with a drift time of ~10 ms (Figure 8a). From the IMS drift time vs. m/z two-dimensional plot, fragments originating from only doubly charged ions are extracted allowing a deconvolution from fragments originating from singly charged ions. Using the deconvoluted MS/MS spectra, the presence of CL can be confirmed based on fragment ions. Figure 8b shows an MS/MS example of $[M-2H]^{2-}$ precursor ion at 723.9 m/z which corresponds to the CL 72:8. Examining the extracted spectra, four main fragment peaks can be observed. The first peak has a m/z of 279.1 which corresponds to the linoleic FA 18:2. Second peak has a m/z of 415.1 which corresponds to the monoacylglycerol phosphate and the third and fourth peaks are masses of 583.4 m/z and 1167.8 m/z corresponding to doubly and singly charged MLCL, respectively. It can be said that these four fragment MS/MS peaks are characteristic of each cardiolipin species, and their structures are shown in (Figure 8c).

CLs due to their complex structure can be isomeric, such as CL (16:1/18:1/ 18:1/ 10:0) and CL (16:1/18:1/ 16:1/ 12:0), meaning they have the same molecular formula (both are CL 62:3), but they have different acyl chain structures (Figure 9a). Therefore, the MS/MS spectrum confirmation and structure characterization can sometimes be more challenging. Such is the example of the MS/MS spectrum of two isomeric 62:3 CL ions at 658.5 m/z

(Figure 9b). The main aspect of this MS/MS spectrum is the presence of four peaks corresponding to four different FAs (18:1 at 281.2 m/z, 16.1 at 253,2 m/z, 12:0 at 199.1 m/z, and 10:0 at 171.1 m/z). Knowing that these four different FAs are originating from precursor CL 62:3 ions at 658.5 m/z, there must be a possible combination of these FAs that are structuring CL 62:3. Doing simple summing, (16:1/18:1/ 18:1/ 10:0) and (16:1/18:1/ 16:1/ 12:0) are only two combinations possible that add up to 62:3. This can be additionally confirmed by observing at the generated singly charged MLCL fragments from spectrum (Figure 9c). The four red highlighted peaks are corresponding to singly charged MLCLs with their possible structures based on detected FAs in (b) spectrum. CL 62:3 has a mass of 1318.9u and a mass peak at 1145.8 m/z is MLCL, a CL (16:1/18:1/18:1/ 10:0) that fragmented FA 10:0 (171.1 m/z). Likewise, the mass peak at 1117.7 m/z is MLCL, a CL (16:1/18:1/16:1/ 12:0) that fragmented FA 12:0 (199.1 m/z). The mass peak at 1063.7 m/z corresponds to two structurally different MLCLs, a CL (16:1/16:1/18:1/12:0) and CL (16:1/18:1/18:1/10:0) that both fragmented FA 16:1 (253.2 m/z). The mass peak at 1035.6 m/z also corresponds to two structurally different MLCLs, originating from mentioned CLs that fragmented FA 18:1 (253.2 m/z). This detailed observation of generated fragments allows a solid structural characterization of CL based on MS/MS spectra.
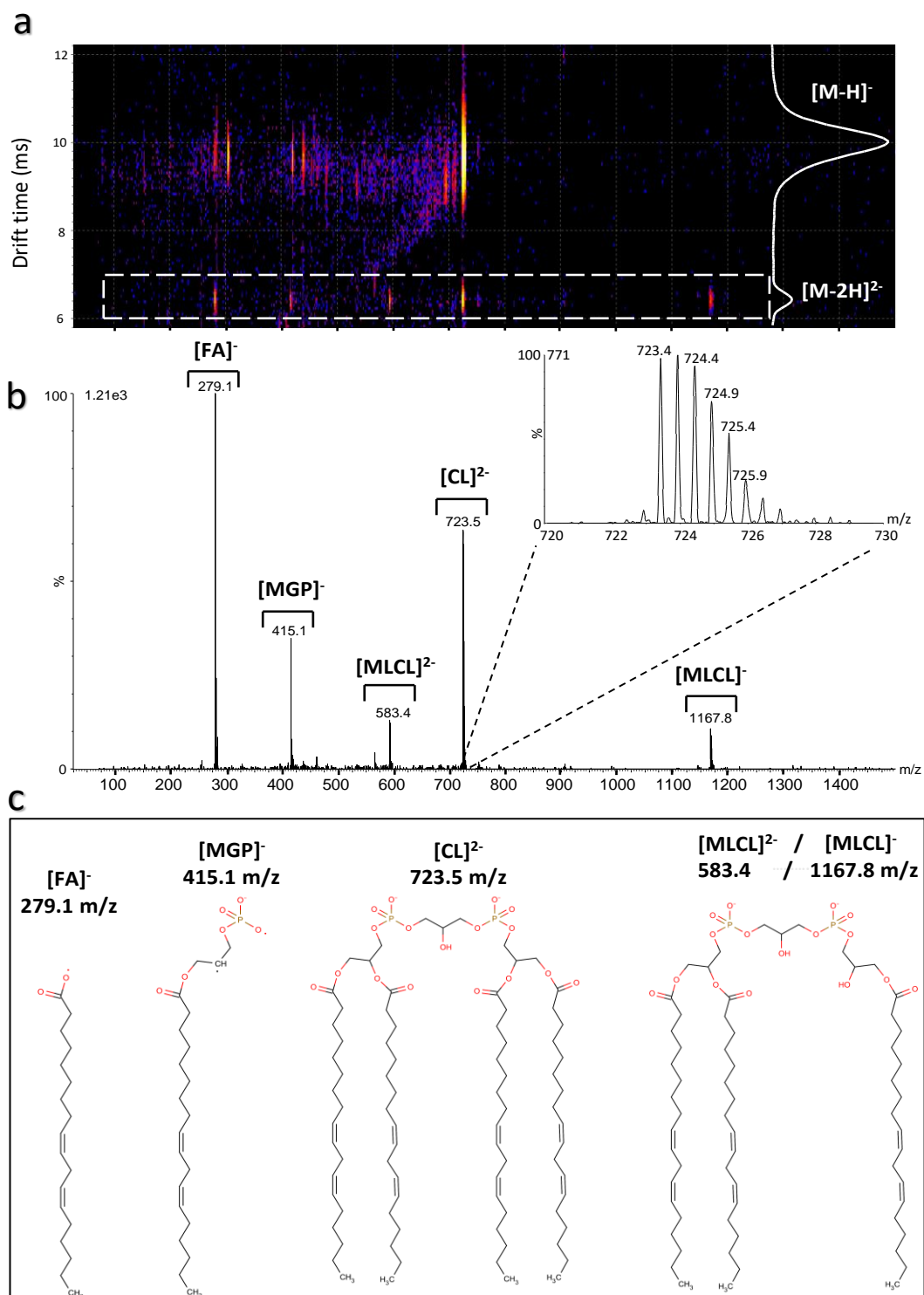
Figure 8. The IMS-MS/MS spectrum of the doubly charged [M-2H]$^{2-}$ CL ion at m/z 723.9. (a) IMS drift time vs. m/z two-dimensional plot showing separation of fragments originating from singly charged ions from fragments originating from doubly charged ions, shown in Drift scope software. **(b)** Isolated MS/MS spectrum of fragments of the doubly charged

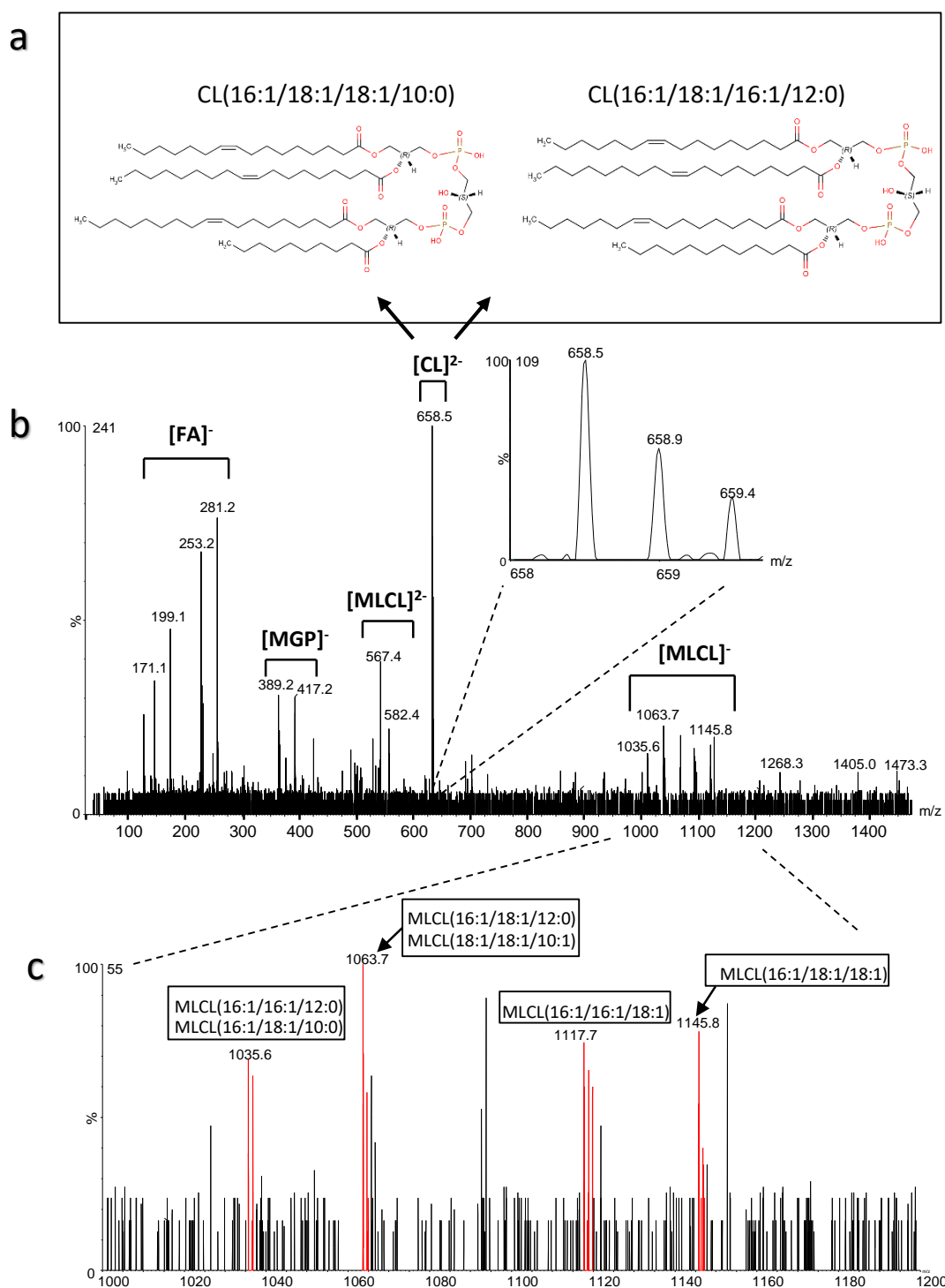ion at 723.9 m/z. **(c)** The structures of CL (72:8) fragments match the m/z's from (b) spectrum.

Figure 9. CL confirmation and structure characterization of isomeric CL. (a) Structures of two different CL molecules, but with the same m/z of 658.5. **(b)** Extracted MS/MS spectrum of doubly charged ions at 658.5 m/z

with CLs fragments highlighted. **(c)** Spectrum (1000-1300m/z) with 4 different red highlighted peaks corresponding to singly charged MLCLs with their possible structures based on detected FAs in (b) spectrum.

4.4. Mass spectrometry optimization

Several steps of the experimental process were examined to optimize the separation, quantification, and structural characterization of CLs. The first one was an optimization of TEA concentration (Figure 10). We used the TEA base in our samples to help deprotonate the CL molecules during the ionization process. The intensity of 0,16 µM CL (14:0)4 with different TEA concentrations was measured. The results indicate the highest peak intensity of CL with 0.1mM TEA concentration.
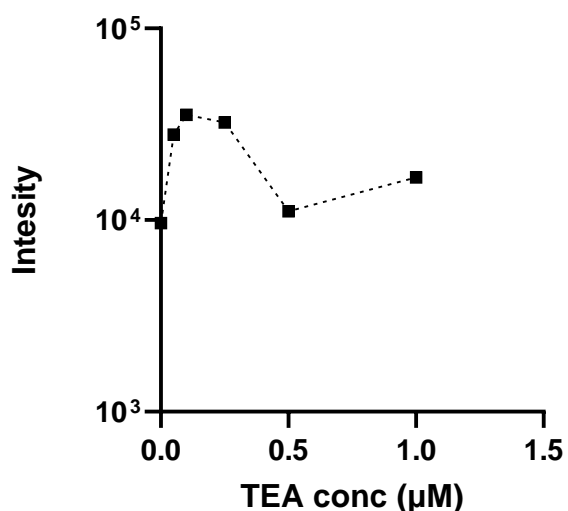
Figure 10. Effect of TEA concentration on CL intensity. The ion intensity of internal standard, CL (14:0)4 (0,16 µM) was determined with different TEA concentrations. The results indicate the highest peak intensity of CL was achieved with 0.01-0.1mM TEA concentration.

Likewise, different instrument parameters were explored to optimize the separation of CLs from singly charged ions. The chronograms and graphs indicate that increases in nitrogen gas flow, helium gas flow, and wave height proportionally increase the distance at which ions are separated (Figure 11).

However, it was also observed how changes in these IMS parameters influenced the signal intensity of CLs (Figure 12). The change in helium gas flow and wave height suggests that there is no significant effect on the CL intensity. On the other hand, when gradually increasing nitrogen gas flow from 20 mL/min to 60 mL/min, there is a clear increase in CL intensity, followed by a plateau at 70 mL/min and a subsequent decrease in CL intensity. Moreover, it was found that the CL intensity is influenced by the DC voltage applied to helium. The results indicate a progressive increase in CL intensity as the DC is raised to 100 V, followed by a subsequent decrease as the applied voltage is further increased. Using the Nanoflow ionization method, nitrogen gas flow and helium DC have been shown to have a similar influence on CL intensity, with optimal intensities at 60mL/min and 100 V, respectively (Figure 13).
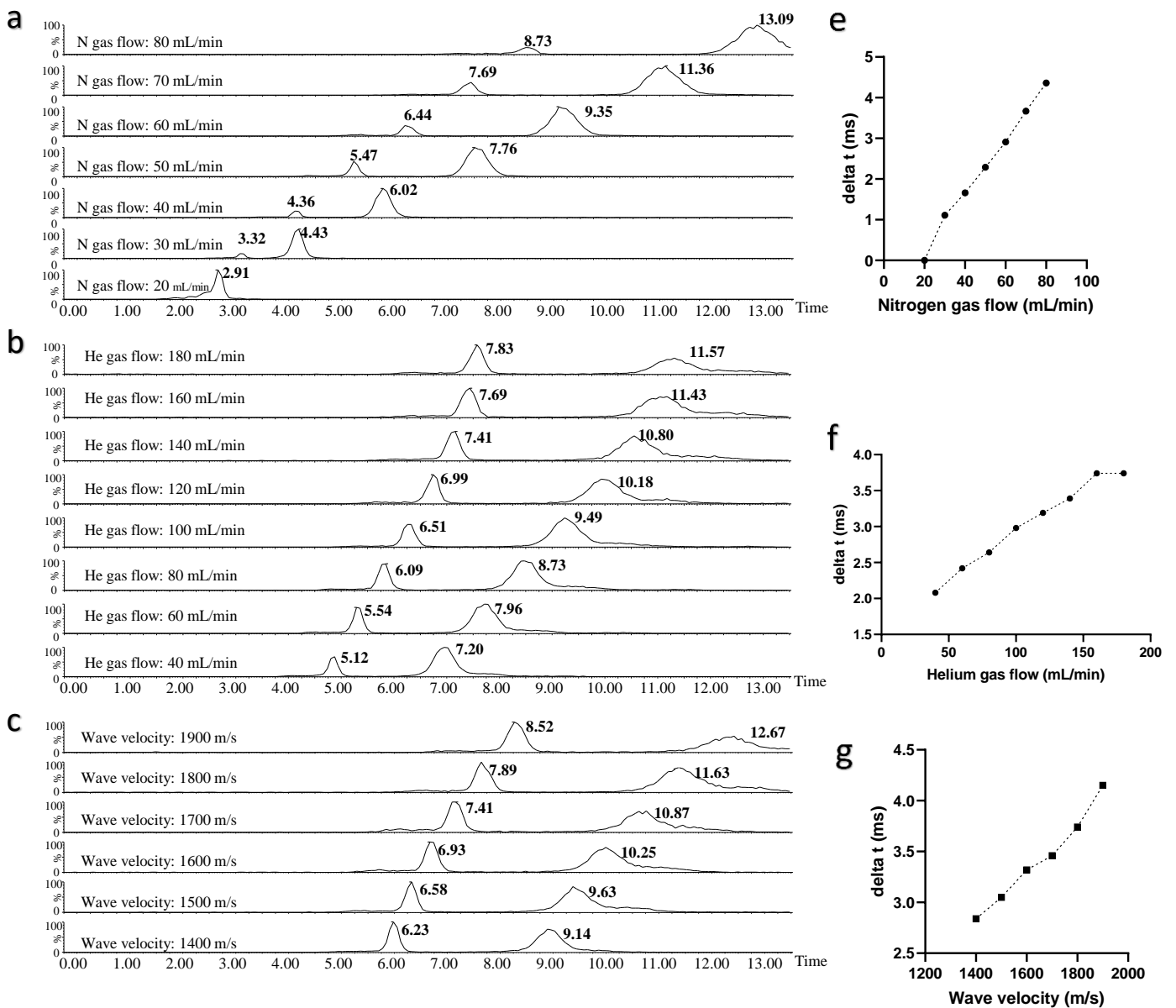
Figure 11. IMS separation of singly charged ions from doubly charged CL ions is altered by IMS instrument parameters. (a), (e) Influence of nitrogen gas flow on IMS separation. **(b), (f)** Influence of helium gas flow on IMS separation. **(c), (g)** Influence of wave velocity on IMS separation. (a,b,c) show IMS drift time chronograms and (d,e,f) show graphs with the difference in speed between singly charged and doubly charged ions.
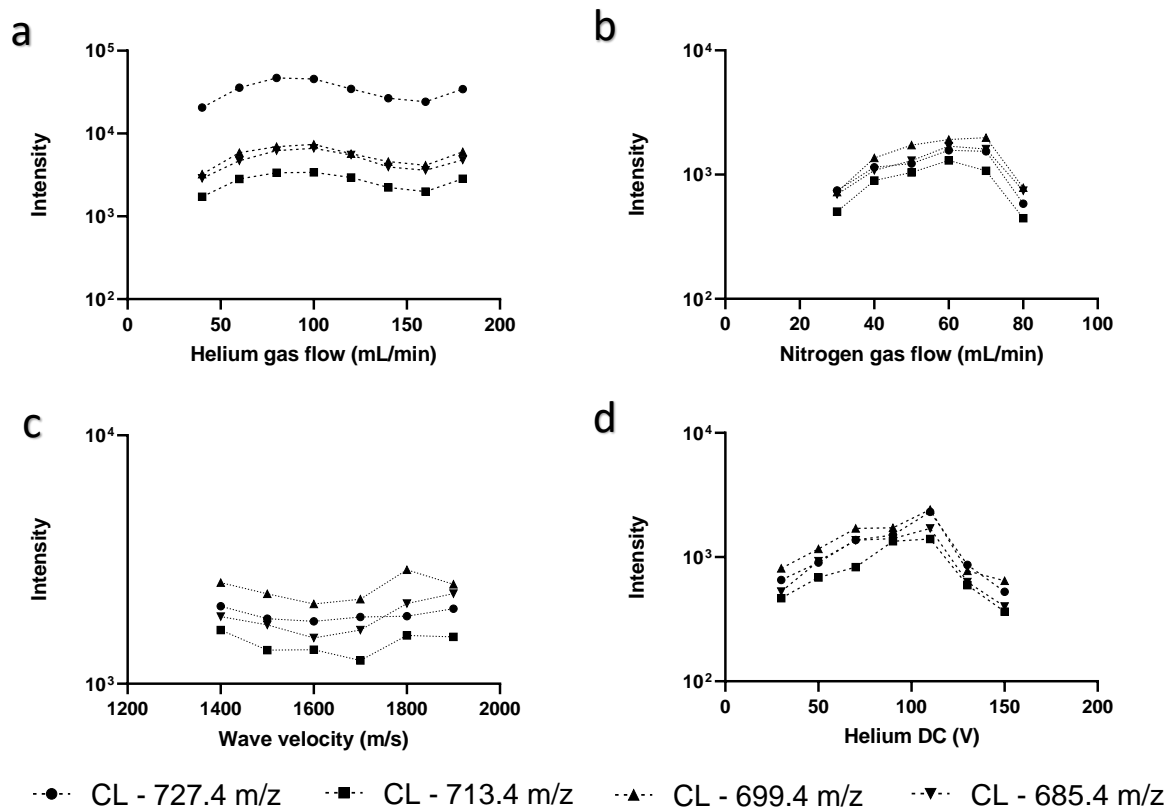
Figure 12. CL signal intensity is influenced by IMS instrument parameters, nitrogen gas flow and helium DC, but not helium gas flow and wave velocity (using ESI). The effect of **(a)** helium gas flow, **(b)** nitrogen gas flow, **(c)** wave velocity, **(d)** and helium DC voltage on CL signal intensity with ESI ionization method. 4 different doubly charged CLs were measured 72:8 (727.4 m/z), 70:4 (713,4 m/z), 68:4 (713,4 m/z), and 64:4 (685,4 m/z)
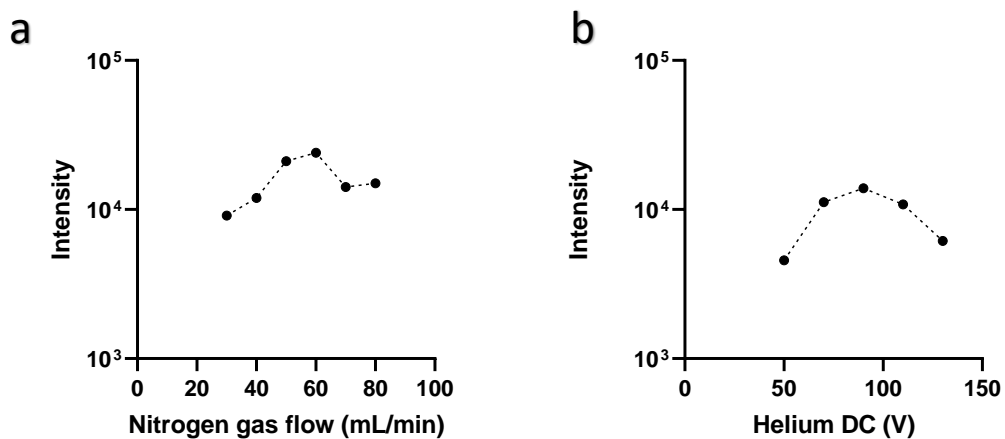
Figure 13. CL signal intensity is influenced by IMS nitrogen gas flow and helium DC voltage (using Nanoflow). **(a)** Nitrogen gas flow **(b)** helium DC voltage change influence on CL signal intensity using Nanoflow ionization method. The intensity of CL $(14:0)_4$ was measured.
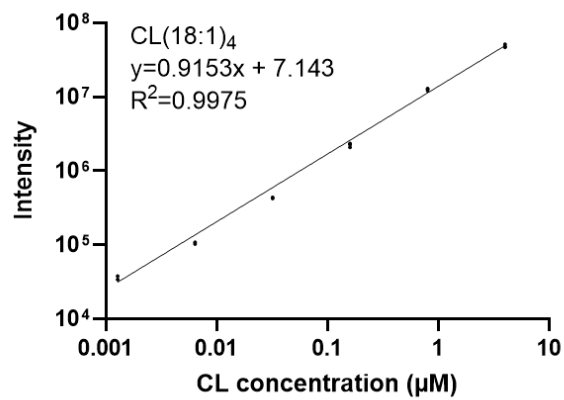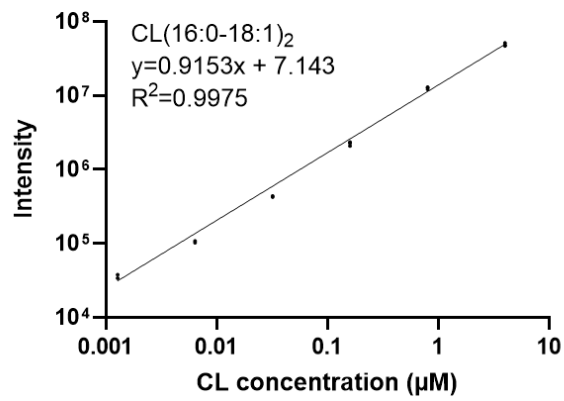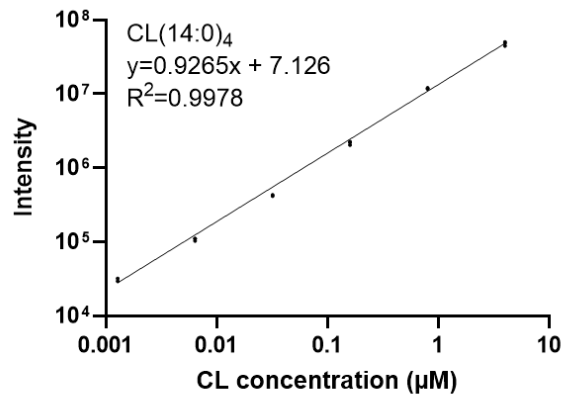
Figure 14. Linear range. Standard dilution series of CL $(14:0)_4$, CL $(16:0\text{-}18:1)_2$ and CL $(18:1)_4$ were linear below 10 µM.

MS/MS analysis can vary significantly based on the voltage applied to fragment precursor ions. Therefore, optimization of ETD voltage for accurate structural characterization and confirmation of CL was required (Figure 15). At 22.5 V, it is clear that fragment intensity levels are low and almost no fragmentation is done. The voltage is too low and higher energy is required to fragment CL. At 25 V, the 279.1 m/z peak, corresponding to FA 18:2 is increased, while other fragments are still low and the precursor ion has the strongest intensity. At 27.5 V, however, the peak intensity of other fragments is increased such as at 415.1 m/z corresponding to the monoacylglycerol phosphate, and peaks at 592.3 m/z and 1167.6 m/z corresponding to doubly and singly charged MLCL, respectively. Increasing velocity after 30V, the precursor ion is overly fragmented, and its peak intensity is starting to get too low. Therefore, the ETD velocity used for all CL fragmentations was set at 28V, where all fragments show a strong intensity.
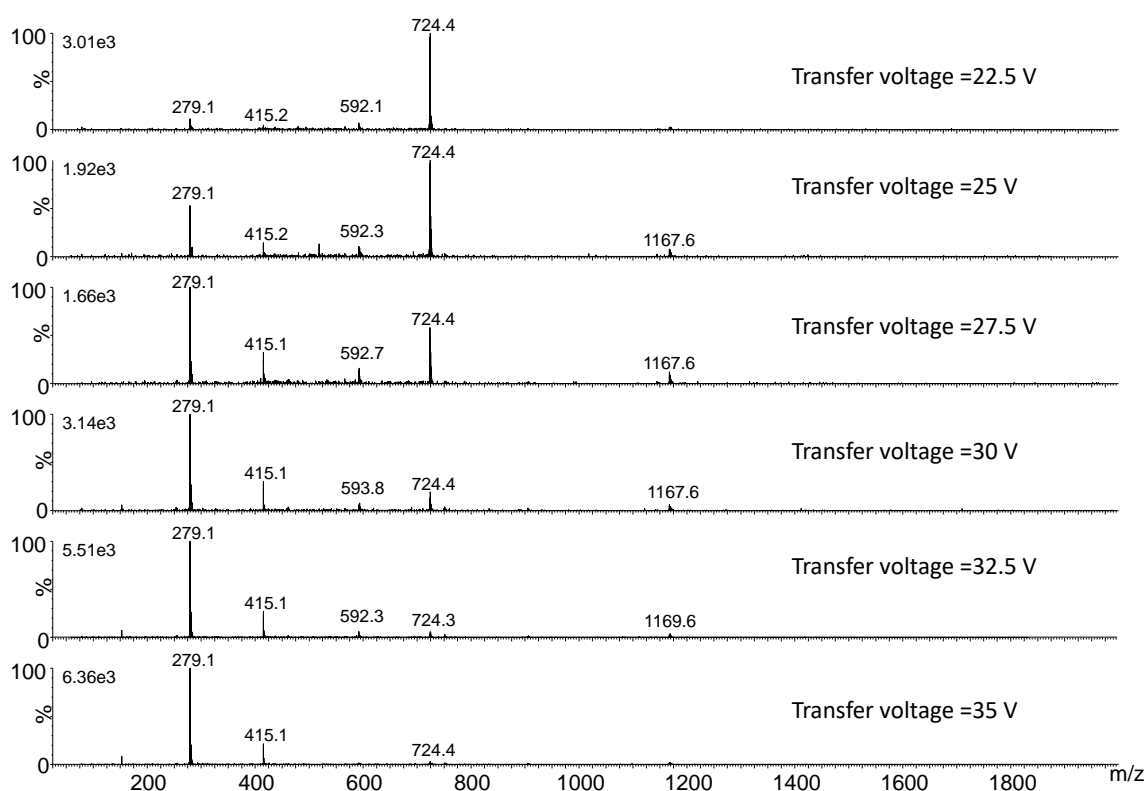

Figure 15. MS/MS spectra of CL 72:4 fragmentation using different ETD voltages. The 279.1 m/z peak corresponds to FA 18:2, 415.1 m/z

peak corresponds to the monoacylglycerol phosphate, and peaks at 592.3 m/z and 1167.6 m/z correspond to doubly and singly charged MLCL.

4.5. CL profiles analysis of CL remodelling mutants in yeast and WT

After optimising the intensity, separation, and fragmentation, we were interested in comparing the CL profiles of yeast WT and the mutant *Cld1ΔTaz1Δ* (which affects the CL remodelling pathway) (Figure 16). Separated and deconvoluted spectra of WT yeast cell in the early stationary phase (24 hours) has the highest peaks in the range of CLs 72: x. Also, looking at the enlarged spectra of CLs 68:x range (698 m/z to 702m/z) it can be noticed that the highest peak intensity has CL 68:4 (699.5 m/z) and the isotopic distribution has a shape appearance like it is the only CL species in that range (Figure 16a). On the other hand, the separated and deconvoluted spectra of the *Cld1ΔTaz1Δ* yeast cell in the early stationary phase (ESP) have the highest peaks in the range of CLs 66: x. it also clears in the enlarged spectra of CLs 68:x range that the highest peak intensity has CL 68:2 (699.5 m/z) and the isotopic distribution has a shape appearance like it is not the only CL species in that range (Figure 16b). To visualize this difference in CL profiles, another Python script was used to generate the graph characterized by carbon chain length and a number of double bonds, where dot size corresponds to abundance relative to total CL content. After the MS/MS analysis and confirmation of each CL, the graphs were used to visualize the CL profiles of WT (Figure 16c) and *Cld1ΔTaz1Δ* mutant (Figure 16d). Using the generated table of corrected CL MI isotopic peaks, the percentage of double bonds number in the total CL profile for WT (Figure 16e) and *Cld1ΔTaz1Δ* (Figure 16. f) is shown by a pie chart. The results show that in ESP, 71.76% of total WT yeast CLs have four double bonds, while only 3.69% of CLs in *Cld1ΔTaz1Δ* have four double bonds. In *Cld1ΔTaz1Δ,* on the other hand, 51.50% of CLs have two double bonds, while in WT they were not even detected in this case. Finally, the comparison, in average carbon chain length and (Figure 16g) average

double bonds (Figure 16h) is shown using a bar graph. The results show that CLs of WT yeast during ESP have on average more double bonds (3.5) than *Cld1ΔTaz1Δ* (1.95)*. Likewise, WT yeast CLs are on average having more carbons (66.2) than *Cld1ΔTaz1Δ* (64.9)*.

We were also interested in comparing the CL profiles of yeast WT and the *Taz1Δ* mutant, which mutation is known to cause Barth syndrome in humans. WT spectrum has also been shown to have CLs with more double bonds and carbons (Figure 17a) than the *Taz1Δ* spectrum (Figure 17b). Most importantly, however, the biggest difference in CL profile between samples is in MLCLs (*m/z* 500-625 range) amount. *Taz1Δ* spectrum has much bigger intensities of MLCLs compared to WT, which can also be seen in the IMS drift time chronogram of WT (Figure 17c) and *Taz1Δ* (Figure 17d) samples. The separation of CL from MLCL is also possible with IMS where MLCLs have drift times between 4.35-5.15 milliseconds, while the CL have drift times between 5.15-6.25 milliseconds. Using the total intensity of MLCL and CL from the chronogram, the ratio of CL against MLCL can be determined (Figure 17e.) and the results show that MLCL: CL ratio in *Taz1Δ* almost 4 times higher than in WT.
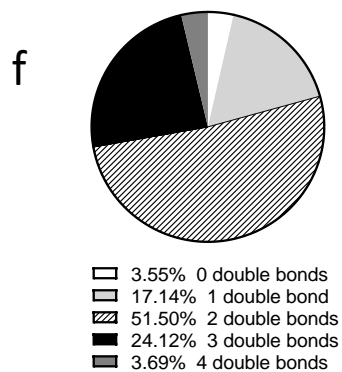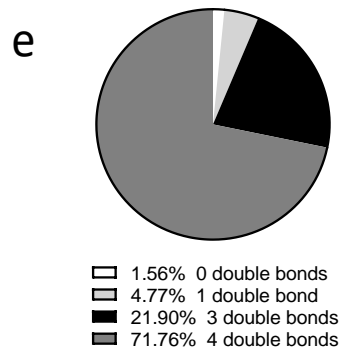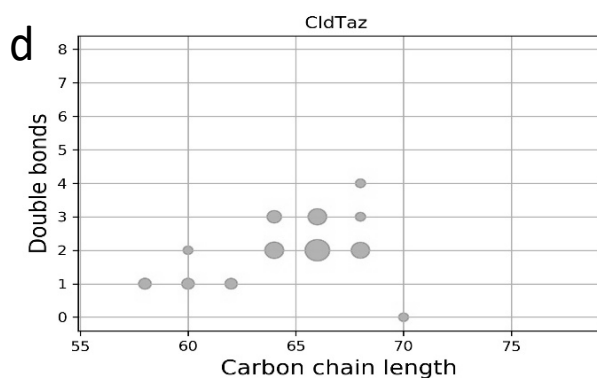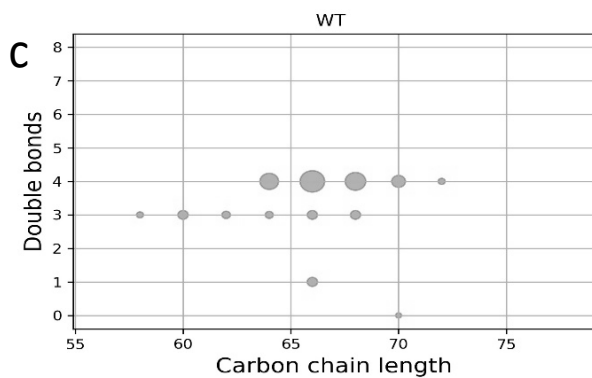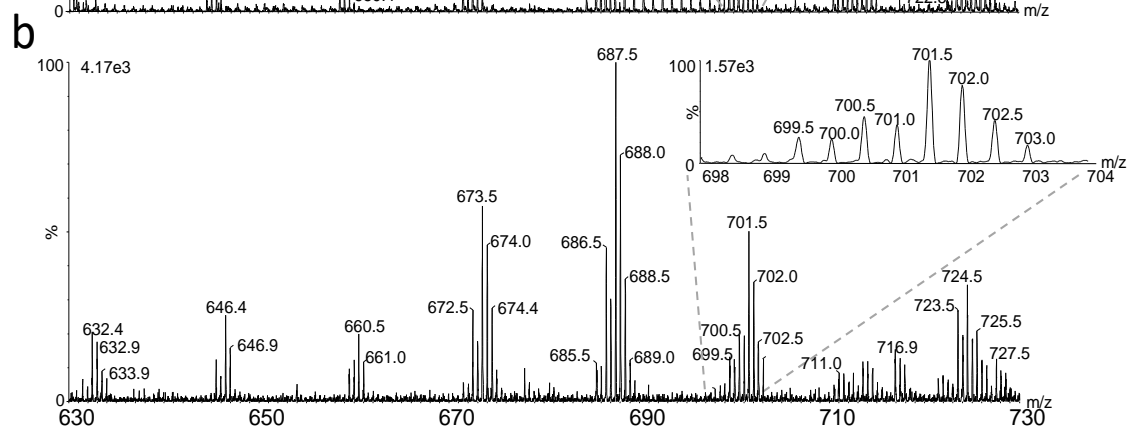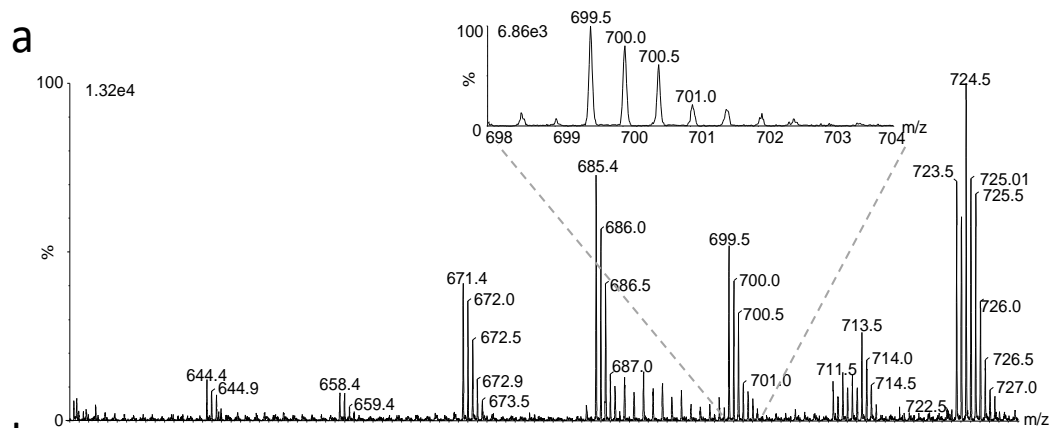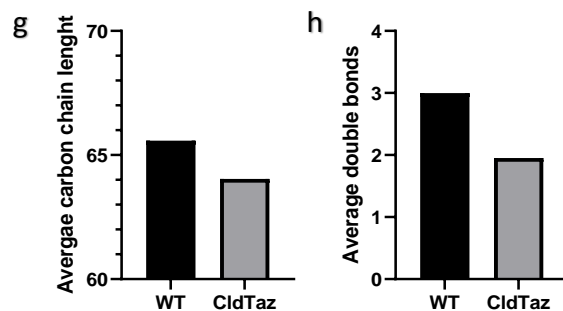
Figure 16. Saturation of the CL acyl chains is higher in *Cld1ΔTaz1Δ* double mutants compared to WT cells. Extracted mass spectra of WT (**a**) and *Cld1ΔTaz1Δ* (**b**) double mutant yeast lipid extract in early stationary phase. Inset spectra highlight the isotopic distribution for CL68: x. CL profile quantification for (**c**) WT and (**d**) *Cld1ΔTaz1Δ* double mutant yeast cells, characterized by carbon chain length and number of double bonds. Dot size corresponds to abundance relative to total CL content. Pie chart representing the percentage of a number of double bonds in total CL profile for WT (**e**) and *Cld1ΔTaz1Δ* (**f**) double mutant. (**g-h**) Bar graph of WT and *Cld1Δaz1Δ* average carbon chain length and average double bond content.

Figure 17. *Taz1Δ* **mutation leads to an increase in MLCL accumulation.** An extracted mass spectrum was obtained from WT yeast (**a**) and from *Taz1Δ* yeast mutant (**b**). IMS drift time chronogram of the [M-2H]2- CL and MLCL ions from WT yeast (**c**) and *Taz1Δ* ye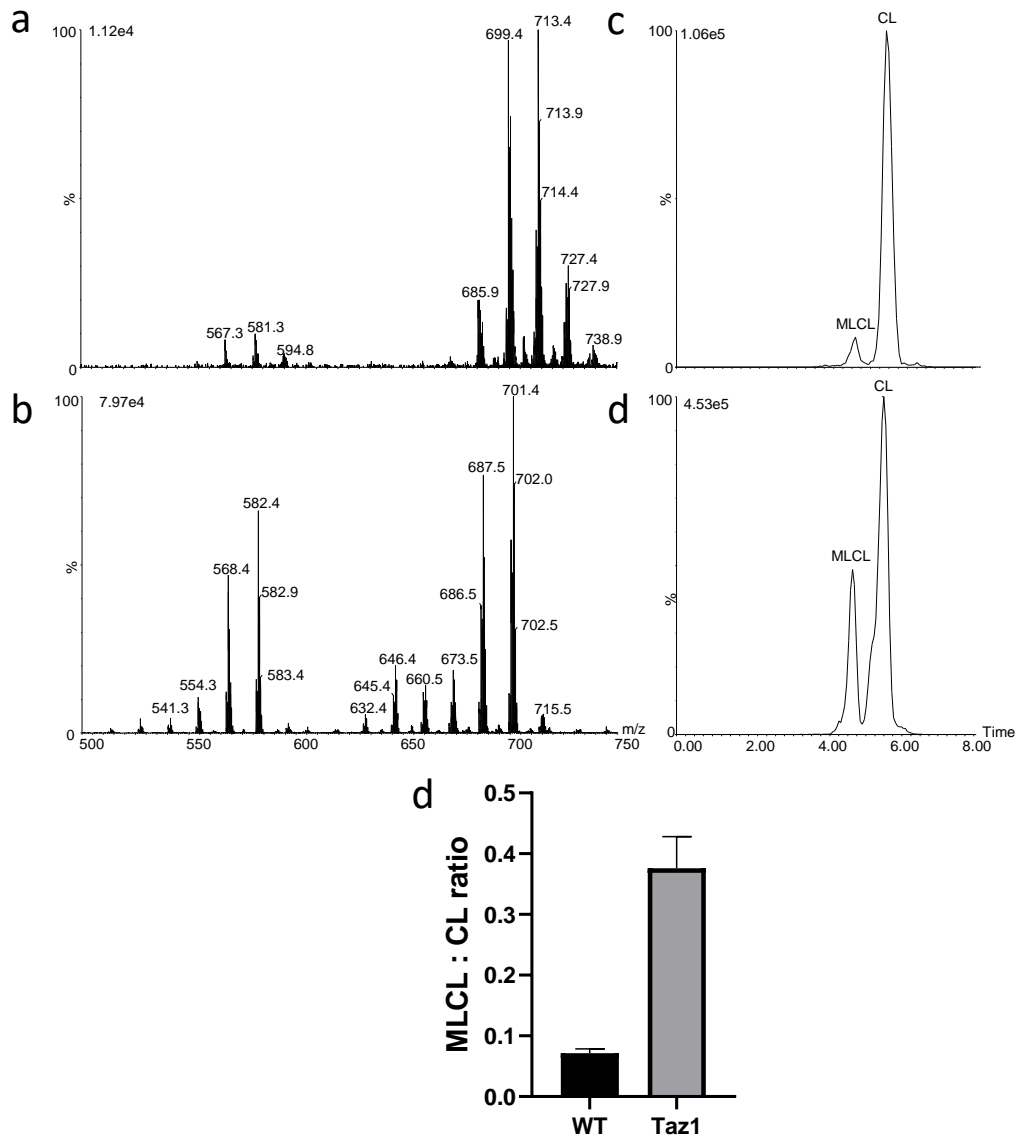ast (**d**). Total MLCL to CL ratio comparison between WT yeast and *Taz1Δ* yeast mutant measured in triplicate (**d**).

4.6. CL profiles analysis of rat organ tissues

The CL profiles of rat mitochondria that had been isolated from the heart, liver, and brain were studied. When examining the mitochondrial heart CL profile (Figure 18a), it appears that just one CL species is largely present and that species is a CL 72:8 (723.7 m/z). The mitochondrial CL profile of the liver displays a little greater diversity of CL species (Figure 18b). In addition to CL 72:8, CL 72:7 (724.7 m/z) appears to be the major CL species in the liver. There are also a few CLs with two carbons fewer or two carbons more than 72, and with different quantities of double bonds. However, when examining the spectra and graph of the brain tissue, an extremely high degree of variety of distinct CL species can be seen (Figure 18c). Some CLs have as little as two double bonds and as many as 12 double bonds and the number of carbon atoms in a CL can also range anywhere from 64 to 78.
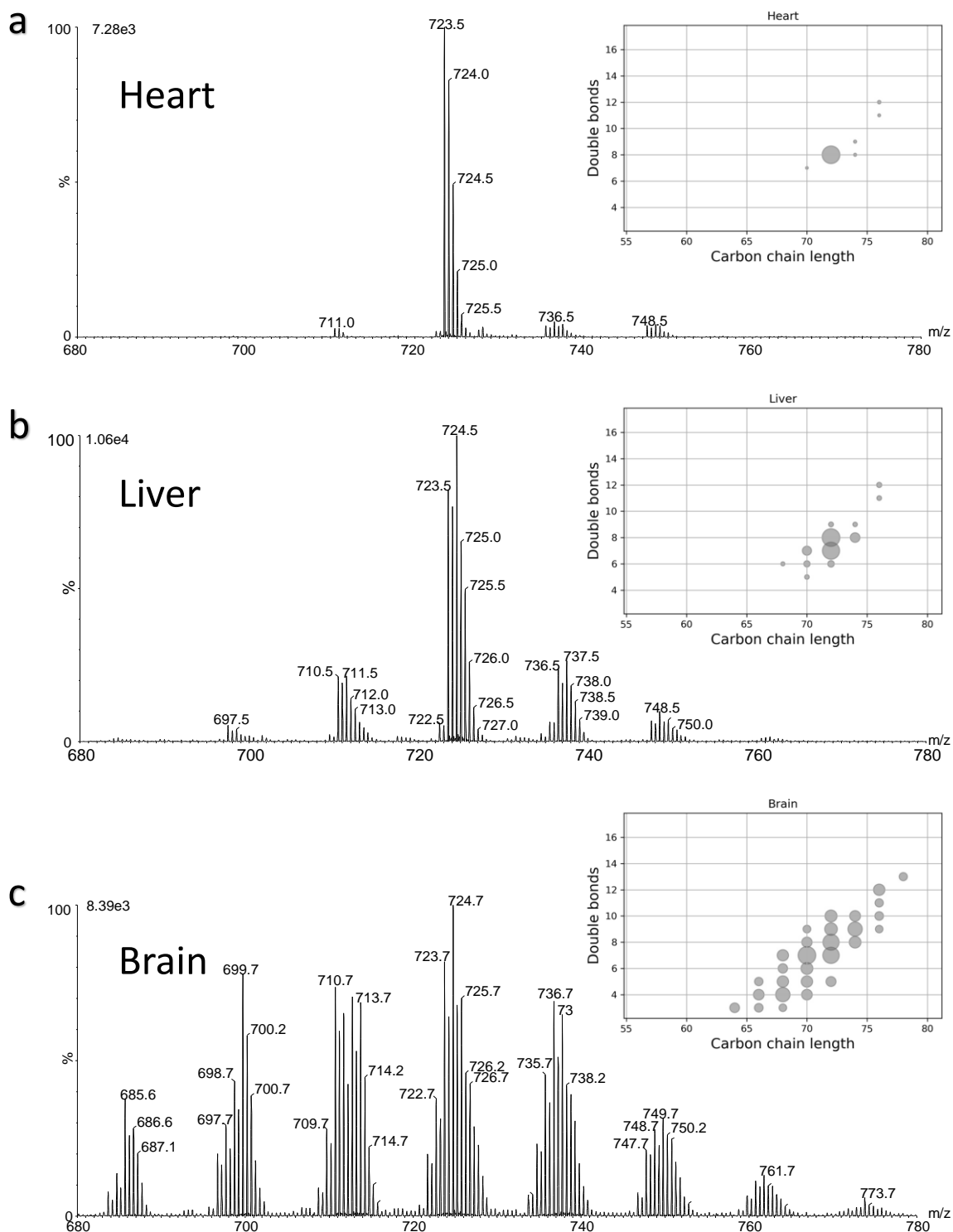
Figure 18. CL profile difference between heart, liver and brain tissue. Extracted mass spectra of rat tissue **(a)** heart, **(b)** liver, **(c)** brain lipid extract. Graph with CL profile quantification is also shown, characterized by carbon chain length and a number of double bonds. Dot size corresponds to abundance relative to total CL content.

5. Discussion

CLs are unique phospholipids found mostly, if not always in the inner mitochondrial membrane of eukaryotes, where they play crucial roles in various cellular processes, including energy production and mitochondrial dynamics (15). Due to their importance, accurately identifying and quantifying CL species is essential for understanding their role in mitochondrial function and interpreting alterations in CL species under pathological conditions. Barth syndrome is a rare genetic disorder characterized by a mutation in the gene coding for tafazzin, an enzyme involved in the cardiolipin remodelling pathway maintaining mitochondrial health and mass spectrometry is a powerful and most common technique used for cardiolipin analysis (10). However, the primary challenge in identifying and quantifying doubly charged CLs using MS is the interference caused by the abundant singly charged ions, masking the intensity signals of doubly charged CLs. This is evident in direct injection spectra of rat liver lipid extracts (Figure 5a.), where the strongest peaks belong to singly charged ions. The strong overlap between singly charge lipid ions, such as phosphatidic acid and doubly charged CL ions makes distinguishing between them difficult. Therefore, an additional separation method of CL from other lipids is required prior to injection to mass spectrometry. Advances in IMS (ion mobility spectrometry) have shown promise in overcoming this limitation. IMS is a gas-phase electrophoretic method that allows ions to be separated in the gas phase based on their shape, charge, and size (40). Doubly charged ions were found to travel more faster through nitrogen gas than singly charged ions, which allowed us to obtain deconvoluted spectrum after IMS separation that showed no unwanted intensities from singly charged ions and revealed the presence of only doubly charged ions. Consequently, IMS enabled us the total separation of doubly charged CL ions, without using LC-MS method and overcoming chromatography matrix effects, which significantly enhanced the accuracy of cardiolipin identification and quantification. We also compared the unseparated and

IMS deconvoluted spectra of a CL $(14:0)_4$ standard. The IMS spectrum shows better peak resolution and lower background noise compared to the raw spectrum. While IMS deconvolution results in a lower overall ion intensity, it improves the signal-to-noise ratio 20-30 times, leading to more reliable and accurate identification of CLs, making it advantageous for precise identification and quantification of CLs at low concentrations.

In this study, we also emphasize the importance of isotopic deconvolution to resolve overlapping peaks caused by isotopes of different CLs with similar masses. Isotopic distribution is a critical aspect of mass spectrometry analysis, especially when dealing with complex lipids like CLs. To accurately quantify CLs, we utilized predicted isotopic distribution calculations with Waters MassLynx software. Based on this data, we developed a correction equation that can be applied to all CL species to account for isotopic overlapping when quantifying CL MI peaks. Automating the peak identification process from spectra is crucial to save time and minimize potential errors inherent in manual approaches. As a result, we developed a Python script capable of automatically detecting peaks corresponding to CLs based on m/z values and calculating MI corrections providing a robust approach for quantifying CLs in complex lipid samples.

After running the Python script, each peak corresponding to a certain CL must be fragmented to confirm whether that peak is due to CL or not. Importantly, in Waters Synapt G2-S, the IMS compartment is placed before the ETD fragmentation cell, enabling IMS to occur before fragmentation, hence fragments ions originating from singly charged ions are also separated from fragments originating from doubly charged ions during MS/MS method. Observing MS/MS spectra not only identifies distinct fragments derived from a CL species but also can determine its precise structure. The fragment we are most interested in to determine CL structure is FA ions. For example, Figure 8 is an MS/MS spectra with the precursor ion at 723.9 m/z corresponding to the CL 72:8 and m/z of 279.1 which corresponds to the linoleic FA 18:2. Based on the fact that CL 72:8 has 4

FAs that in total add up to 72 carbons and 8 double bonds, there should be a possibility of combining fragment FAs that also add up to 72 carbons and 8 double bonds. In this case, there is only one FA ion present meaning that this CL has to be made of four linoleic FA 18:2, which do add up to the number of carbons and double bonds of CL 72:8, confirming the presence and structure of CL. This approach becomes particularly important when dealing with isomeric CLs with the same molecular formula but different acyl chain structures, such as CL (16:1/18:1/ 18:1/ 10:0) and CL (16:1/18:1/ 16:1/ 12:0) in Figure 9.

The study optimizes several experimental parameters to improve the separation, quantification, and structural characterization of CLs. For instance, the concentration of the TEA base was optimized, and different IMS parameters were explored to enhance the separation of CLs and to determine their impact on CL intensity and spectral quality. The concentration of TEA base used for deprotonation during ionization of 0.1mM was optimal for obtaining the highest CL intensity. The increase of nitrogen gas flow, helium gas flow, and wave height, all resulted in a proportional increase in the separation distance of CLs from singly charged ions. Consequently, it became imperative to investigate the impact of these separation parameters on CL intensity detection. Nitrogen gas flow and helium DC voltage influenced the CL intensity, with the optimal intensity achieved at 60 mL/min and 100 V, respectively. The optimized conditions were important for obtaining accurate and reliable results. Helium gas flow and wave velocity did not have a significant effect on CL intensity, so they were set at 120 mL/min and 1600 m/s, respectively, as these resulted in the most centred separation on the graph while visualizing in MassLynx software. We also optimized the MS/MS analysis by adjusting the ETD voltage. The ETD voltage of 28V was found to provide the best fragmentation efficiency, leading to clear and characteristic fragment peaks for each CL species without excessive fragmentation of precursor ions. The size of a molecule can significantly influence its behaviour in mass

spectrometry, particularly in ESI. Our linear range results indicate that using IMS the mass spectrometry response does not decrease linearly with increasing chain length, such as with quantification and LC-MS separation method by Gerret et al. (33)

We also performed a comprehensive comparison of CL profiles in various samples, including yeast WT, mutant *Cld1ΔTaz1*, mutant *Taz1Δ*, and rat tissues (heart, liver, and brain). The CL profiles were compared after optimizing intensity, separation, and fragmentation. The results showed significant differences in the CL composition between yeast WT and mutant *Cld1ΔTaz1*. In the ESP, yeast WT cells had higher peak intensities for CLs with four double bonds, while *Cld1ΔTaz1* mutant cells had more CLs with two double bonds. Additionally, the average carbon chain length and average double bonds were higher in WT yeast compared to the mutant. This confirms previous findings that the enzymes responsible for the *de novo* CL synthesis lack acyl specificity, while the Cld1 enzyme has a greater affinity for saturated acyl chains. As a result, the process of CL remodelling in WT contributes to an increased proportion of unsaturated acyl groups in CLs (42). These findings indicate that the absence of the Cld1 enzyme causes the inability of yeast to start the CL remodelling pathway, as Cld1 is the only CL-specific phospholipase, resulting in *Cld1ΔTaz1* CL profile with only de novo synthesized CLs. The CL profile of WT yeasts was also compared to the CL profile of the *Taz1Δ* mutant, which is known to cause Barth syndrome in people. The results showed that the CL profile was very different between the two strains. Most notably, in contrast to the WT strain, the *Taz1Δ* mutant spectrum had much higher amounts of MLCLs. This elevated buildup of MLCLs indicates a disturbance in the metabolism of CLs and points to a crucial function for tafazzin in maintaining the homeostasis of CLs (43). The big increase (almost 4 times) in the MLCL/CL ratio shows that deacylation is the first step in the process of remodelling and causes a buildup of MLCLs when the tafazzin enzyme is missing to reacylatate CLs. Additionally, the lack of tafazzin caused the number of

unsaturated CLs to go down, as tafazzin usually has a greater affinity towards unsaturated acyl chains (5). In this study, we also examined CL profiles in rat mitochondria from the heart, liver, and brain. The results indicated tissue-specific differences in CL composition. The heart mitochondria predominantly contained CL 72:8, while the liver mitochondria showed more diversity with CL 72:8 and CL 72:7 as major species. However, a wide variety of CL species with variable amounts of double bonds and carbon chain length were present in the brain mitochondria. These results support earlier studies that also showed a non-random distribution of the fatty acyl configuration (7). For example, CL 72:8 was shown to be the dominating species in heart tissue. On the other hand, the ratio of FA18:1 and FA16:1 to FA18:2 was higher in liver tissue, which resulted in a higher abundance of CL 72:7. Without a doubt, the brain tissue exhibited the greatest range of CLs. The composition of CLs is incredibly varied, encompassing molecules with as few as 62 carbons and 2 double bonds, all the way up to those with a staggering 78 carbons and 10 double bonds. These results imply that various tissues have varied requirements for CL composition in order to satisfy their unique functional requirements. However, the unique processes behind the generation and regulation of CL compositions that are tissue-specific remain mostly unknown.

Our future aims are to write a new Python script for automated confirmation of CL based on MS/MS spectra. Furthermore, we aim to compare the WT and remodelling pathway of yeast mutant strains to explore their difference in CL profiles at various growth stages and different carbon sources. It is also possible to use IMS-MS/MS to improve diagnosis methods for Barth Syndrome and understand the disease mechanism in greater detail. The roles of certain CL species in cellular processes, energy metabolism, and disease development may be investigated further to provide a better understanding of the CL profile diversities and possible therapeutic approaches.

Overall, the comparison of CL profiles in various samples provides valuable insights into the diversity of CLs in different cellular contexts. The observed differences in CL composition between mutants and WT, as well as among different tissues, highlight the significance of CLs in cellular function and the potential implications of CL alterations in disease conditions. Understanding CL regulation and dynamics could pave the way for potential therapeutic strategies targeting CL metabolism in various pathological conditions.

6. Conclusion

In conclusion, the study successfully demonstrates the effectiveness of IMS deconvolution in quantifying and characterizing doubly charged CLs, overcoming the challenges posed by interfering with singly charged ions. The application of IMS spectral deconvolution notably improves the signal to noise providing a more accurate representation of their abundance and enabling a deeper understanding of their functional significance. Synapt G2-s with IMS happening before MS/MS fragmentation also allows a simple and detailed understanding of the CL structural characterization as fragments originating from only doubly charged ions are extracted allowing a deconvolution. Moreover, the study presents the importance of isotopic deconvolution to address overlapping CL peak issues in complex lipid analysis. Using predicted isotopic distributions and an innovative Python script, the research developed a robust method for automatic CL peak identification and MI correction, saving time and reducing potential errors in quantification. Moreover, the research delves into the enhancement of experimental parameters to optimize the separation, quantification, and structural characterization of CLs. Through fine-tuning, optimal conditions for ionization, separation, and fragmentation were identified, ensuring reliable and accurate results. Additionally, the study conducts a thorough analysis of CL profiles across diverse samples, including yeast mutants and rat tissues. This analysis reveals a remarkable diversity in CL profiles, driven by genetic mutations influencing CL remodelling pathways in yeast, as well as the tissue-specific requirements within mammalian tissue. In conclusion, the research not only showcases the effectiveness of IMS deconvolution in addressing challenges posed by interfering ions but also highlights the crucial roles of isotopic deconvolution and parameter optimization in advancing lipid analysis. The comprehensive analysis of CL profiles is important for future understating of mysterious, but very important lipids for healthy homeostasis of mitochondria and organisms.

7. Literature

1. Osellame LD, Blacker TS, Duchen MR. Cellular and molecular mechanisms of mitochondrial function. Best Pract Res Clin Endocrinol Metab [Internet]. 2012 [cited 2023 Aug 10];26(6):711. Available from: /pmc/articles/PMC3513836/

2. Dudek J. Role of cardiolipin in mitochondrial signaling pathways. Front Cell Dev Biol. 2017 Sep 29;5(SEP):297929.

3. Wasmus C, Dudek J. life Metabolic Alterations Caused by Defective Cardiolipin Remodeling in Inherited Cardiomyopathies. [cited 2023 Aug 10]; Available from: www.mdpi.com/journal/life

4. Mejia EM, Nguyen H, Hatch GM. Mammalian cardiolipin biosynthesis. Chem Phys Lipids. 2014 Apr 1;179:11–6.

5. Ye C, Shen Z, Greenberg ML. Cardiolipin remodeling: a regulatory hub for modulating cardiolipin metabolism and function. J Bioenerg Biomembr [Internet]. 2016 Apr 1 [cited 2023 Mar 27];48(2):113. Available from: /pmc/articles/PMC4449329/

6. Hsu Y-H, Dumlao DS, Cao J, Dennis EA. Assessing Phospholipase A 2 Activity toward Cardiolipin by Mass Spectrometry. PLoS One [Internet]. 2013 [cited 2023 Aug 10];8(3):59267. Available from: www.plosone.org

7. Oemer G, Koch J, Wohlfarter Y, Alam MT, Lackner K, Sailer S, et al. Phospholipid Acyl Chain Diversity Controls the Tissue-Specific Assembly of Mitochondrial Cardiolipins. Cell Rep. 2020 Mar 24;30(12):4281-4291.e4.

8. Vetica F, Sansone A, Meliota C, Batani G, Roberti M, Chatgilialoglu C, et al. Free-Radical-Mediated Formation of Trans-Cardiolipin Isomers, Analytical Approaches for Lipidomics and Consequences of the Structural Organization of Membranes. Biomol 2020, Vol 10, Page 1189 [Internet]. 2020 Aug 15 [cited 2023 Aug 21];10(8):1189. Available from: https://www.mdpi.com/2218-273X/10/8/1189/htm

9. What is Barth Syndrome? : Barth Syndrome : Barth Syndrome Foundation [Internet]. [cited 2023 Aug 18]. Available from: https://www.barthsyndrome.org/barthsyndrome/

10. Clarke SLN, Bowron A, Gonzalez IL, Groves SJ, Newbury-Ecob R, Clayton N, et al. Barth syndrome. Orphanet J Rare Dis [Internet]. 2013 Feb 12 [cited 2023 Aug 10];8(1):1–17. Available from: https://ojrd.biomedcentral.com/articles/10.1186/1750-1172-8-23

11. Gasanoff ES, Yaguzhinsky LS, Garab G. Cardiolipin, Non-Bilayer Structures and Mitochondrial Bioenergetics: Relevance to Cardiovascular Disease. Cells 2021, Vol 10, Page 1721 [Internet].

2021 Jul 8 [cited 2023 Aug 12];10(7):1721. Available from: https://www.mdpi.com/2073-4409/10/7/1721/htm

12. De Kroon AIPM, Rijken PJ, De Smet CH. Checks and balances in membrane phospholipid class and acyl chain homeostasis, the yeast perspective. 2013 [cited 2023 Aug 12]; Available from: http://dx.doi.org/10.1016/j.plipres.2013.04.006

13. Koller D, Lohner K. The role of spontaneous lipid curvature in the interaction of interfacially active peptides with membranes ☆ Keywords: Antimicrobial peptide Membrane interface Membrane curvature Membrane disruption Inverse hexagonal phase Non-lamellar (cubic) phase. 2014 [cited 2023 Aug 17]; Available from: http://dx.doi.org/10.1016/j.bbamem.2014.05.013

14. Thakur R, Naik A, Panda A, Raghu P. Regulation of membrane turnover by phosphatidic acid: Cellular functions and disease implications. Front Cell Dev Biol. 2019 Jun 4;7(JUN):458233.

15. Paradies G, Paradies V, Ruggiero FM, Petrosillo G. Role of Cardiolipin in Mitochondrial Function and Dynamics in Health and Disease: Molecular and Pharmacological Aspects. Cells [Internet]. 2019 Jul 1 [cited 2023 Mar 27];8(7). Available from: /pmc/articles/PMC6678812/

16. Ott M, Zhivotovsky B, Orrenius S. Role of cardiolipin in cytochrome c release from mitochondria. Cell Death Differ. 2007 Jul;14(7):1243–7.

17. Animal and Cellular Models of Barth Syndrome : Research : Barth Syndrome Foundation [Internet]. [cited 2023 Aug 12]. Available from: https://www.barthsyndrome.org/research/animalandcellularmodelsofbarthsyndrome.html

18. Xu Y, Zhang S, Malhotra A, Edelman-Novemsky I, Ma J, Kruppa A, et al. Characterization of Tafazzin Splice Variants from Humans and Fruit Flies. J Biol Chem [Internet]. 2009 Oct 10 [cited 2023 Aug 12];284(42):29230. Available from: /pmc/articles/PMC2781466/

19. Pu WT. Experimental Models of Barth Syndrome. J Inherit Metab Dis [Internet]. 2022 Jan 1 [cited 2023 Aug 12];45(1):72. Available from: /pmc/articles/PMC8814986/

20. Xu Y, Anjaneyulu M, Donelian A, Yu W, Greenberg ML, Ren M, et al. Assembly of the complexes of oxidative phosphorylation triggers the remodeling of cardiolipin. Proc Natl Acad Sci U S A [Internet]. 2019 Jun 6 [cited 2023 Aug 12];166(23):11235–40. Available from: /pmc/articles/PMC6561273/

21. Bautista JS, Falabella M, Flannery PJ, Hanna MG, Heales SJR, Pope SAS, et al. Advances in methods to analyse cardiolipin and their

clinical applications. TrAC Trends Anal Chem. 2022 Dec 1;157:116808.

22. Glish GL, Vachet RW. The basics of mass spectrometry in the twenty-first century. Nat Rev Drug Discov 2003 22 [Internet]. 2003 Feb [cited 2023 Aug 11];2(2):140–50. Available from: https://www.nature.com/articles/nrd1011

23. Ho CS, Lam CWK, Chan MHM, Cheung RCK, Law LK, Lit LCW, et al. Electrospray Ionisation Mass Spectrometry: Principles and Clinical Applications. Clin Biochem Rev [Internet]. 2003 [cited 2023 Aug 11];24(1):3. Available from: /pmc/articles/PMC1853331/

24. Dass C. Fundamentals of Contemporary Mass Spectrometry. Fundam Contemp Mass Spectrom [Internet]. 2007 Apr 13 [cited 2023 Aug 11]; Available from: https://onlinelibrary.wiley.com/doi/book/10.1002/0470118490

25. Kaklamanos G, Aprea E, Theodoridis G. Mass Spectrometry: Principles and Instrumentation. Encycl Food Heal. 2016 Jan 1;661–8.

26. Haag AM. Mass analyzers and mass spectrometers. Adv Exp Med Biol [Internet]. 2016 [cited 2023 Aug 13];919:157–69. Available from: https://link.springer.com/chapter/10.1007/978-3-319-41448-5_7

27. Gross JH. Tandem Mass Spectrometry. Mass Spectrom [Internet]. 2017 [cited 2023 Aug 13];539–612. Available from: https://link.springer.com/chapter/10.1007/978-3-319-54398-7_9

28. Minkler PE, Hoppel CL. Separation and characterization of cardiolipin molecular species by reverse-phase ion pair high-performance liquid chromatography-mass spectrometry. J Lipid Res [Internet]. 2010 Apr 1 [cited 2023 Aug 13];51(4):856–65. Available from: http://www.jlr.org/article/S002222752030496X/fulltext

29. Sparagna GC, Johnson CA, McCune SA, Moore RL, Murphy RC. Quantitation of cardiolipin molecular species in spontaneously hypertensive heart failure rats using electrospray ionization mass spectrometry. J Lipid Res. 2005 Jun 1;46(6):1196–204.

30. Wang YJ, Jackson SN, Woods AS. Direct MALDI-MS Analysis of Cardiolipin from Rat Organs Sections.

31. Valianpour F, Wanders RJA, Barth PG, Overmars H, Van Gennip AH. Quantitative and Compositional Study of Cardiolipin in Platelets by Electrospray Ionization Mass Spectrometry: Application for the Identification of Barth Syndrome Patients. Clin Chem [Internet]. 2002 Sep 1 [cited 2023 Mar 27];48(9):1390–7. Available from: https://academic.oup.com/clinchem/article/48/9/1390/5642377

32. Han X, Yang K, Yang J, Cheng H, Gross RW. Shotgun lipidomics of cardiolipin molecular species in lipid extracts of biological samples. J

Lipid Res [Internet]. 2006 [cited 2023 Mar 27];47(4):864. Available from: /pmc/articles/PMC2147724/

33. Garrett TA, Kordestani R, Raetz CRH. Quantification of Cardiolipin by Liquid Chromatography-Electrospray Ionization Mass Spectrometry. Methods Enzymol. 2007 Jan 1;433:213–30.

34. Lange M, Ni Z, Criscuolo A, Fedorova M. Liquid Chromatography Techniques in Lipidomics Research. Chromatogr 2018 821 [Internet]. 2018 Nov 16 [cited 2023 Mar 27];82(1):77–100. Available from: https://link.springer.com/article/10.1007/s10337-018-3656-4

35. Oemer G, Lackner K, Muigg K, Krumschnabel G, Watschinger K, Sailer S, et al. Molecular structural diversity of mitochondrial cardiolipins. Proc Natl Acad Sci U S A [Internet]. 2018 Apr 17 [cited 2022 May 9];115(16):4158–63. Available from: www.pnas.org/lookup/suppl/doi:10.

36. Hu C, Duan Q, Han X. Strategies to improve/eliminate the limitations in shotgun lipidomics. Proteomics [Internet]. 2020 Jun 1 [cited 2023 Aug 13];20(11):e1900070. Available from: /pmc/articles/PMC7394605/

37. Han X, Yang K, Yang J, Cheng H, Gross RW. Shotgun lipidomics of cardiolipin molecular species in lipid extracts of biological samples. J Lipid Res [Internet]. 2006 [cited 2023 Aug 13];47(4):864. Available from: /pmc/articles/PMC2147724/

38. Gao F, McDaniel J, Chen EY, Rockwell HE, Nguyen C, Lynes MD, et al. Adapted MS/MSALL Shotgun Lipidomics Approach for Analysis of Cardiolipin Molecular Species. Lipids [Internet]. 2018 Jan 1 [cited 2023 Aug 13];53(1):133. Available from: /pmc/articles/PMC6369710/

39. Ramani Venkata A, Ramesh M. A concise review on lipidomics analysis in biological samples. ADMET DMPK [Internet]. 2021 [cited 2023 Aug 13];9(1):1. Available from: /pmc/articles/PMC8923307/

40. Dodds JN, Baker ES. Ion Mobility Spectrometry: Fundamental Concepts, Instrumentation, Applications, and the Road Ahead. J Am Soc Mass Spectrom [Internet]. 2019 Nov 1 [cited 2023 Aug 13];30(11):2185–95. Available from: https://pubs.acs.org/doi/full/10.1007/s13361-019-02288-2

41. Wildgoose JL, Richardson K, Green M. TWO DIMENSIONAL MS-MS ON A Q-TOF UTILISING A SCANNING QUADRUPOLE MASS FILTER AND AN ULTRA FAST DATA ACQUISITION SYSTEM OVERVIEW PURPOSE: A novel data-independent acquisition mode suitable for implementation on Q-ToF and Trap-ToF instruments is demonstrated.

42. Baile MG, Sathappa M, Lu YW, Pryce E, Whited K, McCaffery JM, et al. Unremodeled and remodeled cardiolipin are functionally

indistinguishable in yeast. J Biol Chem [Internet]. 2014 Jan 17 [cited 2022 May 9];289(3):1768–78. Available from: https://pubmed.ncbi.nlm.nih.gov/24285538/

43. Ye C, Lou W, Li Y, Chatzispyrou IA, Hüttemann M, Lee I, et al. Deletion of the cardiolipin-specific phospholipase Cld1 rescues growth and life span defects in the tafazzin mutant: implications for Barth syndrome. J Biol Chem [Internet]. 2014 Feb 7 [cited 2022 May 9];289(6):3114–25. Available from: https://pubmed.ncbi.nlm.nih.gov/24318983/